STRATIGRAPHY, MAJOR OXIDE GEOCHEMISTRY, AND $^{40}Ar/^{39}Ar$ GEOCHRONOLOGY OF A TEPHRA SECTION NEAR TOK, ALASKA

By

Janet R. Guidetti Schaefer

RECOMMENDED:

Advisory Committee Chair

Chair, Department of Geology and Geophysics

APPROVED:

Dean, College of Science, Engineering, and Mathematics

Dean of the Graduate School

11-21-02

Date

STRATIGRAPHY, MAJOR OXIDE GEOCHEMISTRY, AND $^{40}Ar/^{39}Ar$ GEOCHRONOLOGY OF A TEPHRA SECTION NEAR TOK, ALASKA

A

THESIS

Presented to the Faculty

of the University of Alaska Fairbanks

in Partial Fulfillment of the Requirements

for the Degree of

MASTER OF SCIENCE

By

Janet R. Guidetti Schaefer, B.S.

Fairbanks, Alaska

December 2002

Abstract

Stratigraphy, major oxide geochemistry, and $^{40}Ar/^{39}Ar$ geochronology are used to describe a tephra section near Tok, Alaska, north of the Wrangell volcanic field. This tephra section contains seven type II tephras and two type I tephras. Hornblende in a tephra near the base of the section was dated at 627.5 +/- 47.7 ka using the $^{40}Ar/^{39}Ar$ method of single-step total laser fusion. This hornblende-rich tephra is here named the Tetlin Tephra. The age and composition of the Tetlin Tephra indicates that it is likely the product of an explosive phase of activity of Mount Drum volcano, where petrologically similar domes were emplaced 650 to 400 ka. Two widespread tephras, the Old Crow Tephra and the Sheep Creek Tephra are also found at this site. The documentation of these tephras combined with the lithologic descriptions provide valuable information for interpretation of the Pleistocene history of this part of interior Alaska.

Table of Contents

List of Figures

List of Tables

List of Appendices

Acknowledgments

Funding for this thesis project was provided by the Alaska Volcano Observatory, a joint program of the United States Geological Survey, the Geophysical Institute of the University of Alaska Fairbanks, and the Alaska Division of Geological and Geophysical Surveys. I gratefully acknowledge my advisors, Dr. Jim Begét, Dr. Paul Layer, and Dr. John Eichelberger for their patient and continuous guidance throughout my years as a graduate student. Special thanks is due to Dr. Chris Nye of the Alaska Volcano Observatory for his encouragement, support, and active enthusiasm on my road to thesis completion. Jeff Drake at the geochronology lab at the University of Alaska Fairbanks provided many hours of helpful instruction. I appreciate the dedication of Ken Severin who gave selfless hours of help with the microprobe.

Chapter 1: Introduction

1.1 Purpose and Scope

Correlation of tephra beds throughout the interior of Alaska and the Yukon is critical to the development of a time-stratigraphic framework for numerous geologic and palynologic studies such as those involving glacial history, climate change, and volcanic eruptive histories. Because Pleistocene sedimentary deposits of interior Alaska and the Yukon are often poorly exposed and difficult to access, the discovery and characterization of new tephra sections in these areas is highly valued. The purpose of this study is to provide a time-stratigraphic description and major oxide geochemical characterization of tephras in a loess section near Tok, Alaska, just north of the Wrangell volcanic field. This section spans much of the Pleistocene and provides an important resource for glacial history and climate change studies of interior Alaska.

In Chapter 1, section 1.3, I provide an introduction to previous work by Westgate and others (1985), Westgate and others (1990), Preece (1991), Preece (1997), and Preece and others (1999) that have laid the ground-work for tephra studies in interior Alaska and the Yukon. In Chapter 2, I document and discuss the stratigraphic relationships of the tephra and sediments, and describe unit thicknesses, tephra grain size, morphology, and crystal character. In Chapter 3, I present a geochemical characterization of specific tephras by electron microprobe major oxide analysis. In Chapter 4, I use $^{40}Ar/^{39}Ar$ dating of

hornblendes to define the age of the thickest tephra in the section. In Chapter 5, I combine the data on major oxide geochemistry, mineral composition, glass shard morphology, stratigraphic position, and age to a) correlate some of the tephras in this section with others in interior Alaska and the Yukon, b) provide a lithostratigraphic interpretation, and c) identify possible source vents of the tephras.

1.2 Location of Tephra Section

The tephra section described is located along the Alaska Highway, southeast of Tok, Alaska, and approximately 100 miles north of the Wrangell volcanic field (Figure 1). This road-cut section is located on the north side of the highway, at mile 1,284.6 of Highway 2 (Alaska Highway), about 17 miles east of Tetlin Junction (63.198°N, 142.178°W). At the time of sample collection and site description in June of 1996, the road-cut was well-exposed and easily accessed.

1.3 Introduction to Late Cenozoic Tephra in Interior Alaska

Tephrochronology in interior Alaska and the Yukon has been advanced greatly by the stratigraphic and geochemical descriptions of the ash beds found in the late Cenozoic loess deposits near Fairbanks, Alaska (Preece and others, 1999; Preece and others, 1992; Preece, 1991; Westgate and others, 1985). A brief summary of this previous work is presented here as an introduction to the tephrostratigraphic framework that has been

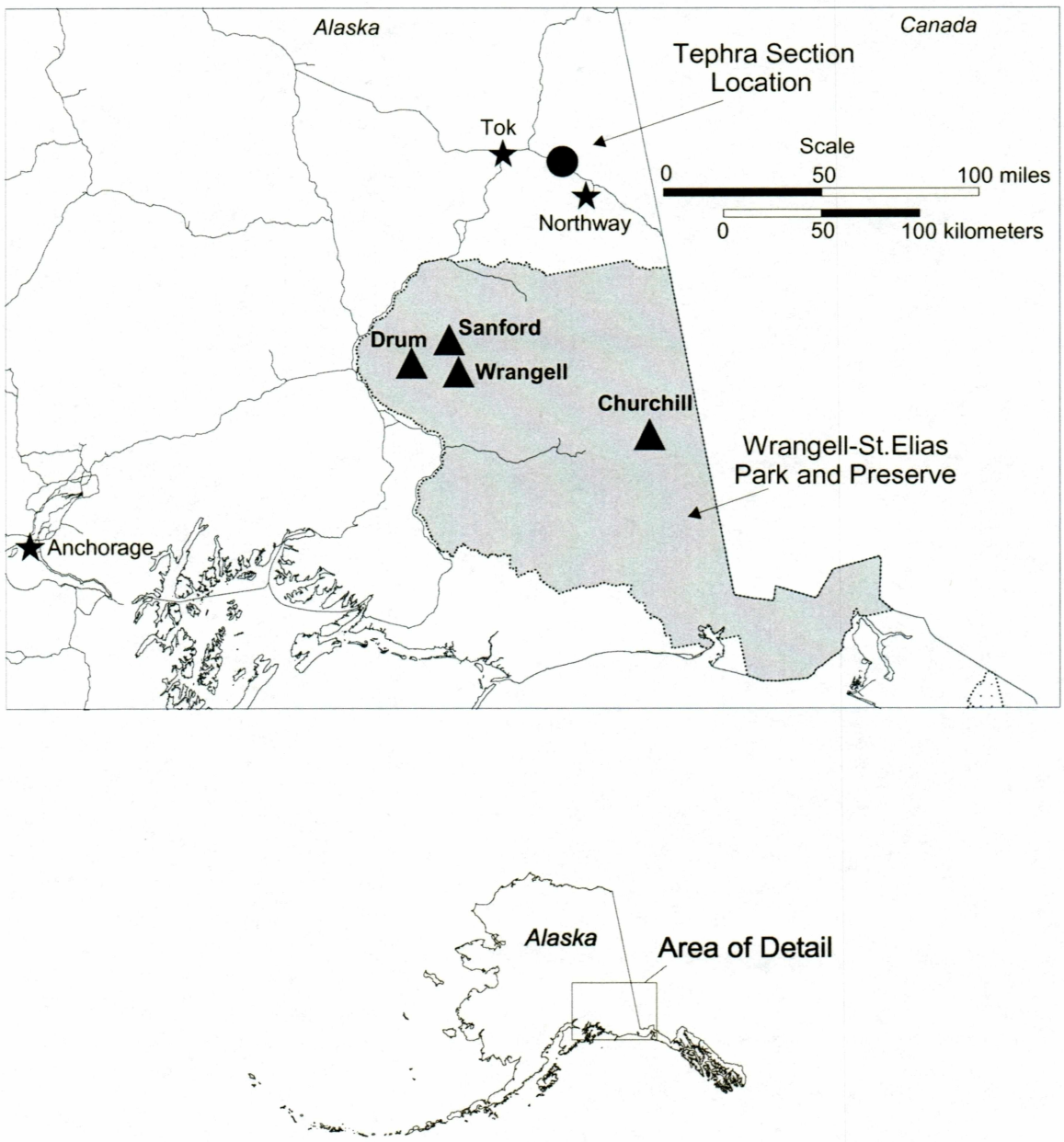

Figure 1: Location of tephra section near Tok, Alaska, north of the Wrangell volcanic field.

established for interior Alaska. Distinguishing characteristics of tephra types are discussed, along with a discussion of source vent candidates.

Three types of tephra have been identified in the Fairbanks area loess based primarily on glass shard morphology and mineral content. Table 1 lists the characteristics of each of the three tephra types. In general, type I glass shards are dominantly bubble-wall or low vesicular pumice and type II glass is mainly frothy pumice. Crystals are rare in type I tephras with clinopyroxene more abundant than hornblende. Type II tephras are hornblende-rich with lesser amounts of clinopyroxene. In addition, Type I tephras have evolved REE profiles while type II tephras have primitive REE profiles. In this thesis, I will document that he Tok area tephra section consists of a series of predominantly type II tephras. Type I tephras are also found at the site, however, type III tephras are not encountered.

Table 1: Summary of tephra types in interior Alaska (modified after Preece, 1991)

Type I	**Type II**	**Type III**
- bubble-wall shards and low vesicular pumice	- highly vesicular pumice	- blocky shards
- clinopyroxene > hornblende	- hornblende >>> clinopyroxene	- biotite >>> hornblende or clinopyroxene
- rare crystals	- abundant crystals	- abundant crystals
- flat REE profiles	- steep REE profiles	- flat REE profile
- low Al_2O_3, CaO	- high Al_2O_3, CaO	- high Al_2O_3
- high FeO, TiO_2	- low FeO, TiO_2	- low FeO, CaO, TiO_2
- low Sr, high Cs, Hf, Sc	- high Sr, low Cs, Hf, Sc	- low Sr, Hf, Sc, very high Cs, Ta

Two potential source regions - the Aleutian-Alaska Peninsula area and the Wrangell volcanic field - have been identified using distinguishing characteristics of type I and type II tephras (Preece and others, 1999). Type I tephras have rhyolitic to dacitic compositions and evolved REE profiles with a well-developed Eu anomaly and La/Yb < 13. This chemical signature is common in high silica volcanic rocks throughout the Aleutians and Alaska Peninsula in places such as Katmai (Hildreth, 1983), Fisher Caldera (Pete Stelling, unpublished data), and Akutan Volcano (Richter and others, 1988). Type II tephras are LREE-encriched with La/Yb > 13. This type of signature is found in rocks of the Wrangell volcanic field, and in particular, Mount Drum (Richter and others, 1994). Only a small part of the Wrangell volcanic field has been studied in detail. Petrologic and geochemical investigations have been conducted at Mount Gordon and Ice Fields Plateau (Richter and Smith, 1976), Mount Drum (Richter and others, 1979; Richter and others, 1990), Skookum Creek (Lowe and others, 1982), Mount Wrangell (Nye, 1983), and Capital Mountain (Richter and others, 1989). The only known proximal samples with dacitic to rhyolitic composition with type II geochemical characteristics are rocks found at Mount Drum and Mount Churchill in the Wrangell volcanic field, and at Hayes volcano in the northeastern portion of the Alaska Peninsula (Preece and others, 1999). Mount Drum and Mount Churchill are the only documented sources of silicic explosive activity in the Wrangell volcanic field that have a type II geochemical signature (Preece, 1997; Westgate and others, 1994).

Chapter 2: Tephra Stratigraphy

2.1 Tephra Stratigraphy at Study Site 96TOK-1

Fourteen tephras are found in a 12-meter-thick section on the north side of the Alaskan Highway, southeast of Tok (Figure 1). Due to extensive glaciation throughout the Pleistocene, few Wrangell area tephras of Pleistocene age are preserved near the volcanoes. This site is highly significant as it reveals over 620,000 years of silt, sand, and tephra accumulation. Nine tephras were analyzed for their major oxide chemistry, using an electron microprobe. The thickest tephra in the section, which occurs in pods from 4- to 16-centimeters-thick near the bottom of the section, was the tephra selected for $^{40}Ar/^{39}Ar$ dating (Chapter 4). Glass morphology and mineral content information for each tephra was combined with the geochemistry and age analyses in an attempt to correlate these tephras with other tephras in interior Alaska (Chapter 5).

The 12-meter-section is dominated by sands and silts with very little preserved organic material. The interbedded sands, silts and tephra beds were deposited against a southeasterly sloping, highly weathered intrusive rock (Figure 2). On the basis of lithology, the section is divided into six units. A generalized stratigraphic column is presented in Figure 3. Most tephras are thin, ranging from 1 mm to 5 cm thick, except for the 4- to 16-cm-thick tephra located near the bottom of the section (Figure 4). Some tephra beds are discontinuous and preserved only as multiple, thin (<1 mm) bands, indicating reworking by wind and/or water.

Figure 2: Road-cut exposure of tephra section 96TOK1. Geologist Jim Begét points to the 4- to 16-cm-thick, hornblende-rich, 96TOK1-9 tephra found near the base of the section.

The approximately 0.5-meter-thick Unit 1 is mainly composed of Holocene loess and soil material, and includes a 2- to 8-cm-thick deposit of the White River Ash, a 1.89 ka common marker bed throughout eastern interior Alaska (Péwé, 1975; Lerbekmo and others, 1975). The recent soil overlies a 23-cm-thick, yellow, cemented, silt bed. Unit 2 is a 2.7-meter section of sand that displays no cross-bedding and only faint parallel bedding. At the base of Unit 2 is a 2-cm-thick unit of granodiorite (?) gravel up to 2 cm in grain size. No tephras are found in Unit 2. Beneath the gravel is Unit 3, consisting of almost a meter of silt and sand. The top 55 cm is composed of silt with sand pods. The lower 40 cm of Unit 3 is composed of sand with finely interbedded silt. At the base of

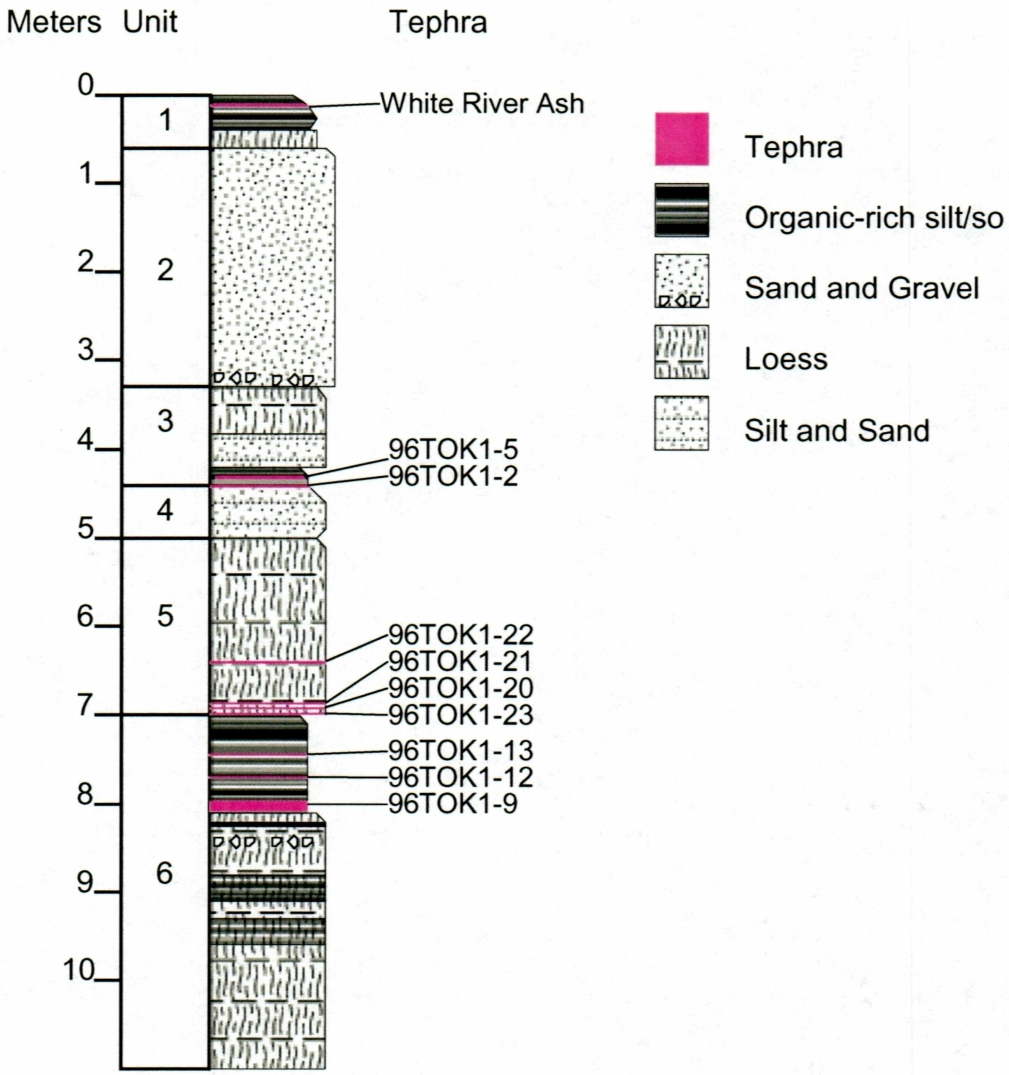

Figure 3: Generalized stratigraphic column showing location of tephra samples.

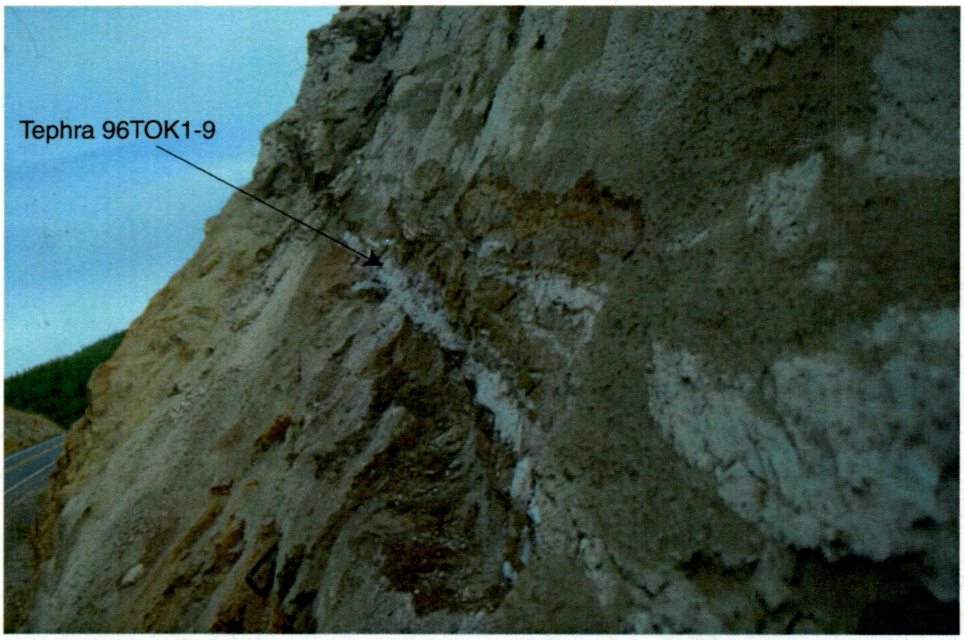

Figure 4: Photograph of 4- to 16cm-thick tephra 96TOK1-9 in the base of the section.

Unit 3, is a 25 cm-thick silty brownish paleosol. Tephra sample 96TOK1-2 was collected within the lower silty soil of Unit 3. Tephra 96TOK1-5 was found as a discontinuous pod slightly up-section and to the east of sample 96TOK1-2. Unit 4 is a 50- to 60-cm-thick layer of silt containing large lenses of sand.

The lower several meters of this outcrop, Units 5 and 6, contain several significant tephras analyzed in this study. Unit 5 is dominated by 2 meters of massive loess. Four tephra samples were collected in this unit: 96TOK1-22, 96TOK1-21, 96TOK1-20, and 96TOK1-23. The top 1 meter of Unit 6 consists of organic-rich, black-gray silt. Within the silt are 1- to 3-cm-thick, organic-rich bands and fine laminations of silt and tephra. Tephra samples 96TOK1-13, 96TOK1-12, and 96TOK1-9 were all

collected within this organic-rich silt unit. Tephra sample 96TOK1-13 occurs as concentrated ash layers within 0.2- to 1-mm-thick laminations of silt and tephra. Fifteen centimeters below this, a sample was taken from an isolated pod of clean, pumiceous, hornblende-rich tephra (96TOK1-12). This same "salt-and-pepper" appearing tephra appears in 4- to 16-cm-thick lenses within organic-rich silt up to 30-cm below 96TOK1-12. The thickest, cleanest sample of this lower, coarse, pumiceous, hornblende-rich tephra was collected for $^{40}Ar/^{39}Ar$ analysis (Tephra 96TOK1-9) (Figure 4).

Unit 6 thickens eastward away from the sloping bedrock surface (Figure 2). The silt contains gravelly to large (up to 10 cm) pieces of granodiorite (?) along with abundant wood particles. A carbon sample was taken here and returned an infinite age (older than approximately 40,000 years). Approximately 1 meter below Tephra 96TOK1-9, there are wispy layers of several multiple-banded tephras. These tephras are very thin and discontinuous and were not looked at in detail for this study.

2.2 Glass Morphology

Seven of the nine tephras analyzed in this study are highly vesicular pumice (Figure 5). The exceptions are tephra 96TOK1-22 and tephra 96TOK1-5 (not pictured) which are characterized by platey, tricuspate bubble-wall shards. Most of the vesicular pumice fragments are about 200 μm across. Tephra 96TOK1-9, however, has an average grain size of about 250 μm. This tephra is the thickest, most coarse-grained tephra in the

section. Most of the platey glass fragments in tephra 96TOK1-22 are less than 100 μm across, with a few that are up to 150 μm.

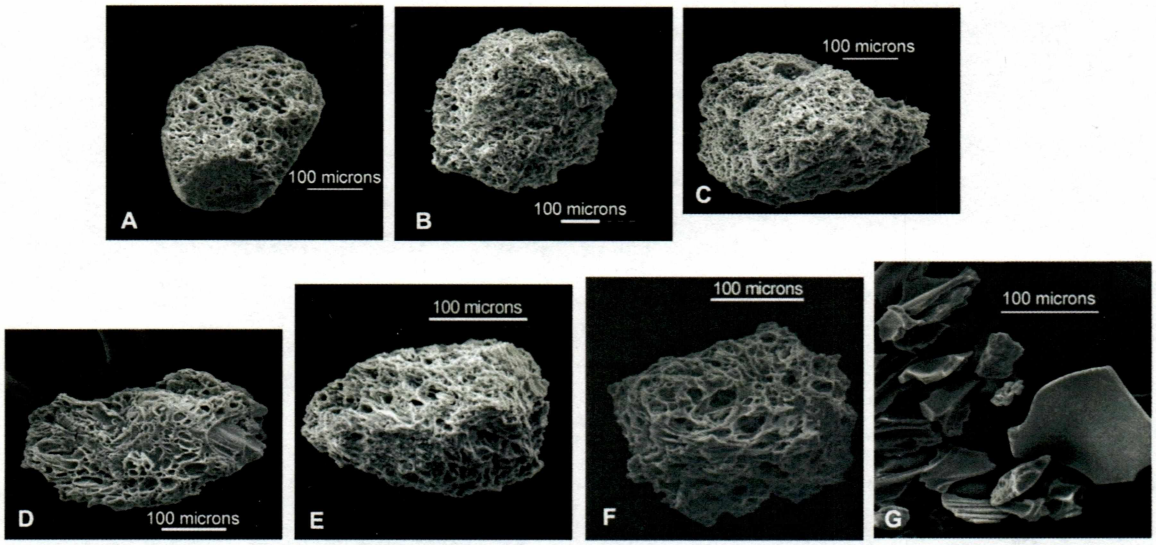

A = 96TOK-1-2; B = 96TOK1-9; C = 96TOK1-12; D = 96TOK1-13; E = 96TOK1-20; F = 96TOK1-21; G = 96TOK1-22

Figure 5: SEM images of tephras collected at site 96TOK1

Chapter 3: Major Oxide Geochemistry

3.1 Introduction

The purpose of this geochemical analysis is twofold. First, hornblende and plagioclase grains from tephra sample 96TOK1-9 were analyzed to determine whether or not multiple populations of these minerals are present in the tephra, the existence of zonation, and their K/Ca ratios. $^{40}Ar/^{39}Ar$ dating requires a general knowledge of the K/Ca ratios of a sample to help constrain the irradiation parameters needed to effectively reduce the interference of K-derived ^{40}Ar and Ca-derived ^{36}Ar in the reactor, yet maximize the production of ^{39}Ar (McDougall and Harrison, 1988; Chapter 4, this study). Second, glass from nine tephras were analyzed for major wt.% oxide concentrations as a first step in chemical characterization that will eventually lead to correlations with other tephras in the vicinity and distal tephras throughout Alaska and the Yukon Territory.

All tephras were collected in June of 1996 from site 96TOK1, a road-cut exposure approximately 17 miles east of Tetlin Junction along the Alaska Highway. Nine of these tephras were prepared for microprobe analysis. Sample 96TOK1-9 is the most coarse-grained of these tephras with visible hornblende grains over 150 μm in size (Figure 6). Hornblende and plagioclase from this tephra and glass shards and pumice fragments from the other tephras were also analyzed.

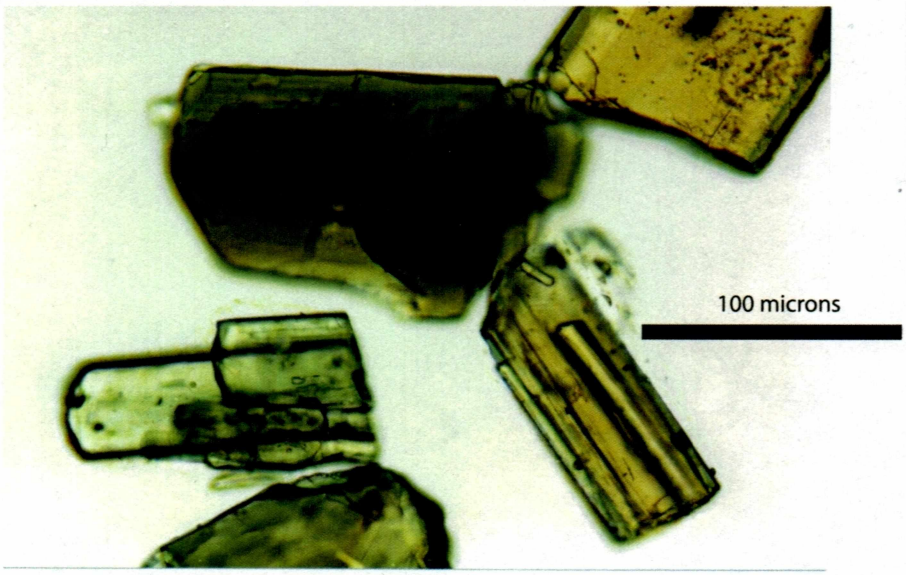

Figure 6: Transmitted light photograph of hornblende in tephra 96TOK-1-9.

3.2 Sample Preparation

Samples were placed in a sonicator and rinsed several times with deionized water to remove fine material. Sodium Polytungstate (SPT) heavy liquid was used to separate glass from heavier minerals. The glass and heavy mineral portions were collected separately by vacuum filtration, washed with deionized water, dried, and mounted on glass slides with epoxy. The mounted slides were ground and polished to expose clean glass or mineral surfaces. The polished surfaces were then cleaned with the commercial glass cleaner Formula 409^{TM} and coated with a carbon layer.

3.3 Electron Microprobe Analytical Procedure

Major element geochemical analyses were performed on a Cameca SX-50 electron microprobe at the University of Alaska, Fairbanks in the Department of Geology and Geophysics in December 1996 and April 1997. Glass samples were analyzed for the nine elements Na, Mg, Al, Si, Cl, K, Ca, Ti and Fe. All elements in the glass analyses except for Cl are reported as weight percent oxides, and all the Fe is reported as Fe_2O_3. Plagioclase grains were analyzed for Na, Al, Si, K, Ca and Fe. Hornblende grains were analyzed for F, Na, Mg, Al, Si, Cl, K, Ca, Ti, Mn and Fe. Standards used for calibration are listed in Appendix I. A 15 kV, 10 nA, 3 μm beam was used for the hornblende and plagioclase. To reduce the effect of Na migration when measuring glass, Na was measured first and the beam size was increased to 10 μm. A ten second counting time was used for all analyses except for Si in glass which was measured for 30 seconds, and Fe and Ti in glass which were measured for 15 seconds. Prior to the analytical session, the electron microprobe was calibrated to within +/- 0.10 wt.% of standard values of the Old Crow tephra for each element analyzed. Working standards for hornblende were Smithsonian Standards HB1 and HB2, and for plagioclase, AN90 and AN70.

Zonation was assessed by probing three points on each hornblende and plagioclase grain in sample 96TOK-1-9, resulting in analyses of the edge, center and mid-point (Appendix III). The mid-point is located between the center of the crystal and the edge. Fourteen grains of hornblende and fifteen grains of plagioclase were chosen at

random for analysis to determine whether or not multiple populations of these crystals exist in this tephra.

Approximately forty points on pumice fragments or glass shards from each sample were probed. Before average wt.% oxides were calculated for each sample, the data was first filtered to remove all totals below 94% and to remove all analyses of minerals such as plagioclase that are often present with the glass.

Detection limits for K and Ca are important in assessing the value of the calculated K/Ca ratios. For hornblende and plagioclase, a K detection limit at the 3σ confidence level can be calculated from the analysis of the standard OR10, and Ca detection limits from analysis of the standard SPHENE1A (Appendix I). At the 3σ confidence level, the detection limit for K is 0.05 wt.% and the detection limit for Ca is 0.06 wt.%.

3.4 Major Oxide Chemistry of Glass

The glass data show a significant range in geochemical composition among all nine samples from site 96TOK1. Wt. % SiO_2 ranges from 69.87 to 75.51, NaO 3.94 to 4.68 wt.%, Al_2O_3 13.42 to 15.04 wt.%, K_2O 2.91 to 3.32 wt.%, CaO 1.54 to 2.44 wt.%, and Fe_2O_3 1.14 to 3.42 wt.% (Appendix II). The tephras are distinguishable, however, and this is especially apparent when the major oxide data is displayed in oxide variation diagrams (Figure 7). Based on glass shard morphology, Al_2O_3 to SiO_2 ratios, and Fe_2O_3 content, both type I and type II tephras are present, although most samples appear to be

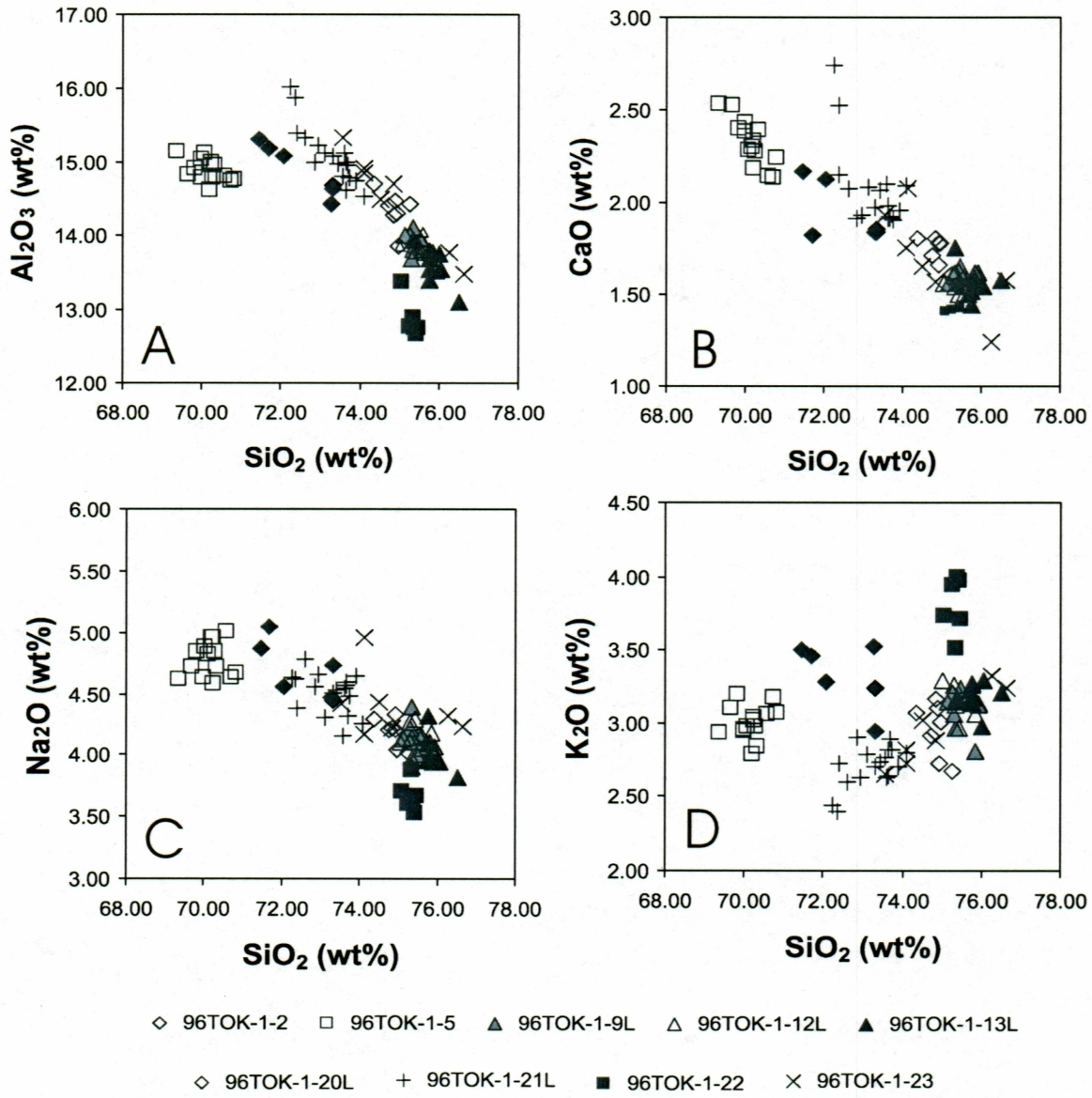

Figure 7: Oxide variation diagrams of glass shard probe analyses from site 96TOK1. (A) SiO_2 vs. Al_2O_3, (B) SiO_2 vs. CaO, (C) SiO_2 vs. Na_2O, (D) SiO_2 vs. K_2O.

type II tephras consisting of highly inflated pumice (Figure 5). Figure 8 illustrates the differences in type I and type II tephras by plotting SiO_2 vs. Al_2O_3 for tephras collected in

this study and type I and type II tephras summarized by Preece and others (1999). Like other type II tephras, the tephras collected at this site have a higher Al_2O_3 content for a given SiO_2 content than the type I tephras. Also the type II tephras have a low Fe_2O_3 content (1.14 to 1.53 wt.%). In contrast, the highest Fe_2O_3 contents of 3.42 wt.% and 1.85 wt.% occur in samples 96TOK1-5 and 96TOK1-22 respectively. Both 1-5 and 1-22 have a bubble-wall shard glass morphology further indicating that these higher Fe tephras are of type I.

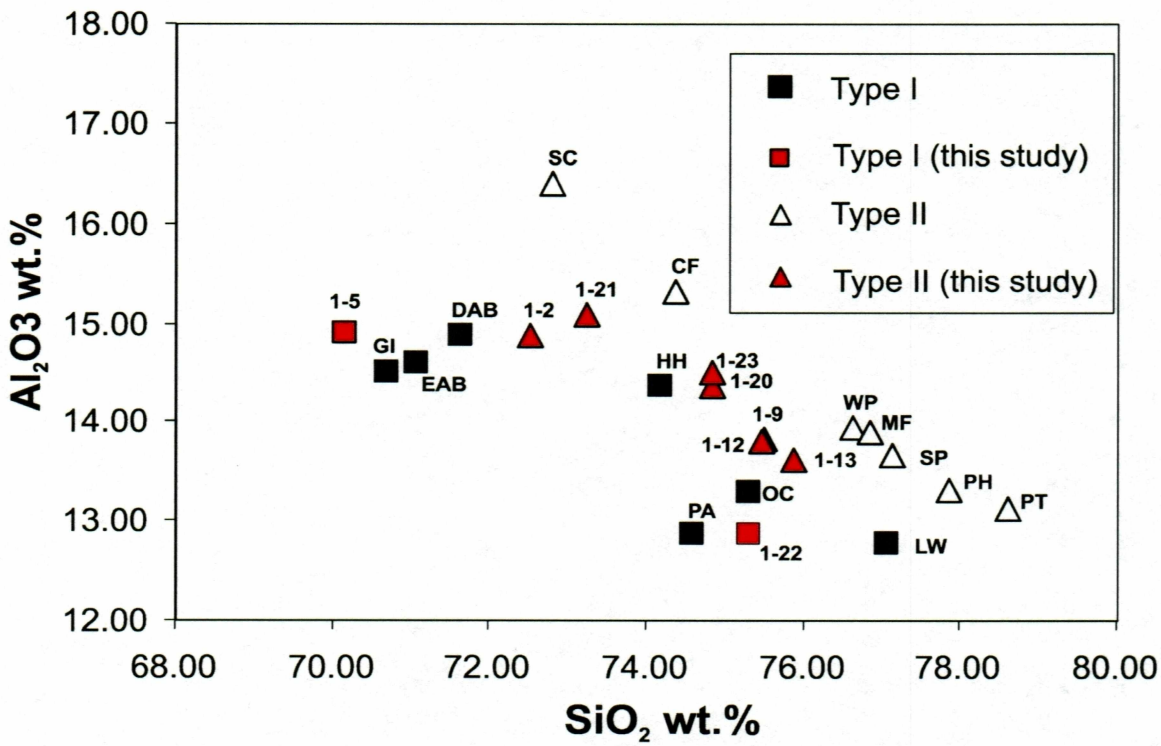

Figure 8: Glass shard SiO_2 vs. Al_2O_3 illustrating the differences in type I and type II tephras. Tephras GI, EAB, DAB, HH, PA, OC, LW, PT, PH, SP, MF, WP, CF, and SC from Preece and others, 1999. Others are average values of tephras collected for this study. For display purposes, the tephra sample labels for this study have been abbreviated by dropping the "96TOK" prefix.

3.5 Hornblende and Plagioclase Crystal Chemistry

Hornblende and plagioclase crystals from sample 96TOK1-9 show no apparent zonation of major cations (Appendix III). Al wt.% oxide shows no systematic variation throughout the hornblende crystal and Ca wt. % oxide shows no systematic variation within the plagioclase. The average wt.% Al_2O_3 for the edge, midpoint (half-way between the edge and center), and center of the fourteen hornblende crystals probed is respectively 10.33 +/- 1.01, 10.09 +/- 0.92, and 10.38 +/- 1.65. The average wt. % CaO for the edge, midpoint, and center of the 15 plagioclase crystals probed are respectively 9.16 +/- 0.87, 9.50 +/- 1.10, and 8.94 +/- 1.13. Thus, the hornblende and plagioclase crystals show a unimodal geochemical distribution, as indicated by the low standard deviation of wt.% oxide for each element within the samples.

The hornblende K/Ca ratio is 0.042. The plagioclase K/Ca ration could not be determined because the amount of K in the plagioclase was below the detection limit of 0.05 wt.% for K. To obtain a better K detection limit, the counting time must be increased. Since the square root of the inverse of the counting time is proportional to detection limit, increasing the counting time increases the detection limit. For the purposes of determining an irradiation parameter for $^{40}Ar/^{39}Ar$ dating, it would be beneficial to be able to detect at least 0.005 wt.% K in order to better resolve the K/Ca ratio. A counting time of 900 seconds (15 minutes) is required to obtain a detection limit of 0.005 wt.% K.

Chapter 4: $^{40}Ar/^{39}Ar$ Dating

4.1 Introduction

Recent advancements in the $^{40}Ar/^{39}Ar$ dating method have pushed the lower limit of age determination into the Pleistocene, especially for ideal candidates such as high K sanidines. Hu and others (1994) reported an $^{40}Ar/^{39}Ar$ age of 12,560 +/- 470 years for sanidines from Mono Craters, California, taking the $^{40}Ar/^{39}Ar$ dating method well into the ^{14}C age range. However, young, fine-grained, low potassium tephra deposits, such as those found in Alaska, pose several problems when applying the $^{40}Ar/^{39}Ar$ dating method. Because of their youth and low original K contents, only small amounts of radiogenic ^{40}Ar are available for measurement thus making corrections for blanks, anomalous atmospheric argon, and interfering irradiation-induced argon isotopes from Ca and K very important. Alteration, weathering, and the intial small grain size of tephras (commonly less than 100 μm) may make them susceptible to the affects of argon recoil. Every correction factor and procedure associated with the $^{40}Ar/^{39}Ar$ dating method must be carefully scrutinized in order to date late Pleistocene, fine-grained, low potassium deposits. Other dating techniques are available for Quaternary tephra (Figure 9), however, the use of the $^{40}Ar/^{39}Ar$ lab at the University of Alaska Fairbanks was chosen in order to make a first attempt at dating less than 1 million-year-old hornblendes in an Alaskan tephra.

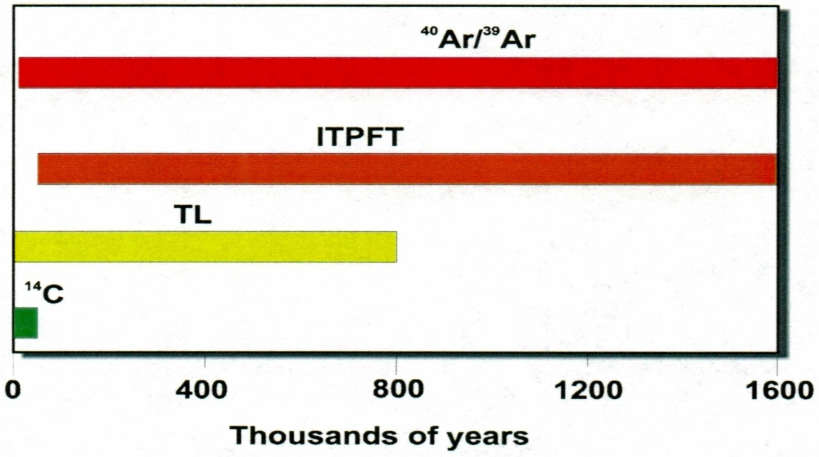

Method	Material	Age Range
$^{40}Ar/^{39}Ar$	Glass, Hornblende, Feldspar	As young as ~13 ka (Hu and others, 1994)
Isothermal Plateau Fission-Track (ITPFT)	Glass shards	~50 ka to 70 Ma (Westgate, pers. commun., 2000)
Thermo-luminescence (TL)	Bracketing Loess	Up to ~800 ka (Berger and others, 1992)
Carbon-14	Peat, Wood, Charcoal	Up to ~40 ka

Figure 9: Quaternary age dating methods.

In this study, the hornblende-rich tephra 96TOK-1-9 was chosen as an ideal candidate to test the limits of the $^{40}Ar/^{39}Ar$ method for such fine-grained, low potassium material. Based on stratigraphic evidence, and an underlying infinite age radiocarbon sample (> 40 ka) the tephra was thought to be about 100,000 years old. Abundant, relatively large hornblende grains are the dominant mineral phase, along with minor plagioclase. Most of the round, frothy pumice grains have a diameter of greater than 250 μm.

4.2 Background Discussion of Optimizing the Precision of the Isotope Intensity Measurement

Age determination of a sample depends on the accuracy of argon isotope ratio measurements (see age equation, Appendix IV, equations A.1 - A.4). Because of the low radiogenic $^{40}Ar^*$ component of young, low-K samples, mass spectrometer measurements become quite sensitive to corrections for blanks, nucleogenic argon isotopes and trapped argon of anomalous isotopic composition.

A major limiting factor in the dating of low $^{40}Ar^*$ samples is the ability to detect a small amount of $^{40}Ar^*$ component above a background of atmospheric argon derived from the sample itself and from the blank of the extraction system (McDougall and Harrison, 1988). Becker and others (1994), have developed an automated resistance furnace, with an infra-red pyrometer, that provides reproducible blanks of $<10^{-16}$ mol for m/e = 40 at 1200° C. Heating time and residence time in the extraction system for gas purification can then be adjusted to minimize the blank contribution, thus optimizing

isotope intensity measurement. They applied this improved blanking system, along with incremental heating, to date basalts with high Ca/K ratios (~25-40), giving isochron ages as young as 409 +/- 18 ka.

The use of a laser as a heat source, rather than a resistance furnace, minimizes the blank contribution even further (York and others, 1981; Layer and others, 1987). The total amount of each argon isotope measured (Ar_m) after irradiation is a sum of naturally occuring isotopes in the sample before irradiation, atmospheric argon (Ar_A), and those generated by the irradiation of K, Ca, and Cl (Ar_A, Ar_{Ca}, and Ar_{Cl}):

$$^{40}Ar_m = {}^{40}Ar^* + {}^{40}Ar_A + {}^{40}Ar_K$$

$$^{39}Ar_m = {}^{39}Ar_K + {}^{39}Ar_{Ca}$$

$$^{38}Ar_m = {}^{38}Ar_A + {}^{38}Ar_{Cl}$$

$$^{37}Ar_m = {}^{37}Ar_{Ca}$$

$$^{36}Ar_m = {}^{36}Ar_A + {}^{36}Ar_{Ca} + {}^{36}Ar_{Cl}$$

These interfering reactions can be minimized by proper choice of irradiation parameter J, related to the irradiation time (Figure 10 and equation A.5, Appendix IV). Minimizing reactor-induced ^{40}Ar from the reaction $^{40}K(n,p)\,^{40}Ar$ relates to the $(^{40}Ar/^{39}Ar)_K$ correction factor (equation A.4, Appendix IV). To ensure the correction factor remains small, such as 1% of the $^{40}Ar^*$, the sample must satisfy the following equation relative to J, the irradiation parameter and t, the age of the sample: $J < (e^{\lambda t} - 1)/100(^{40}Ar/^{39}Ar)_K$. This is shown as the upper limit solid curve in Figure 10.

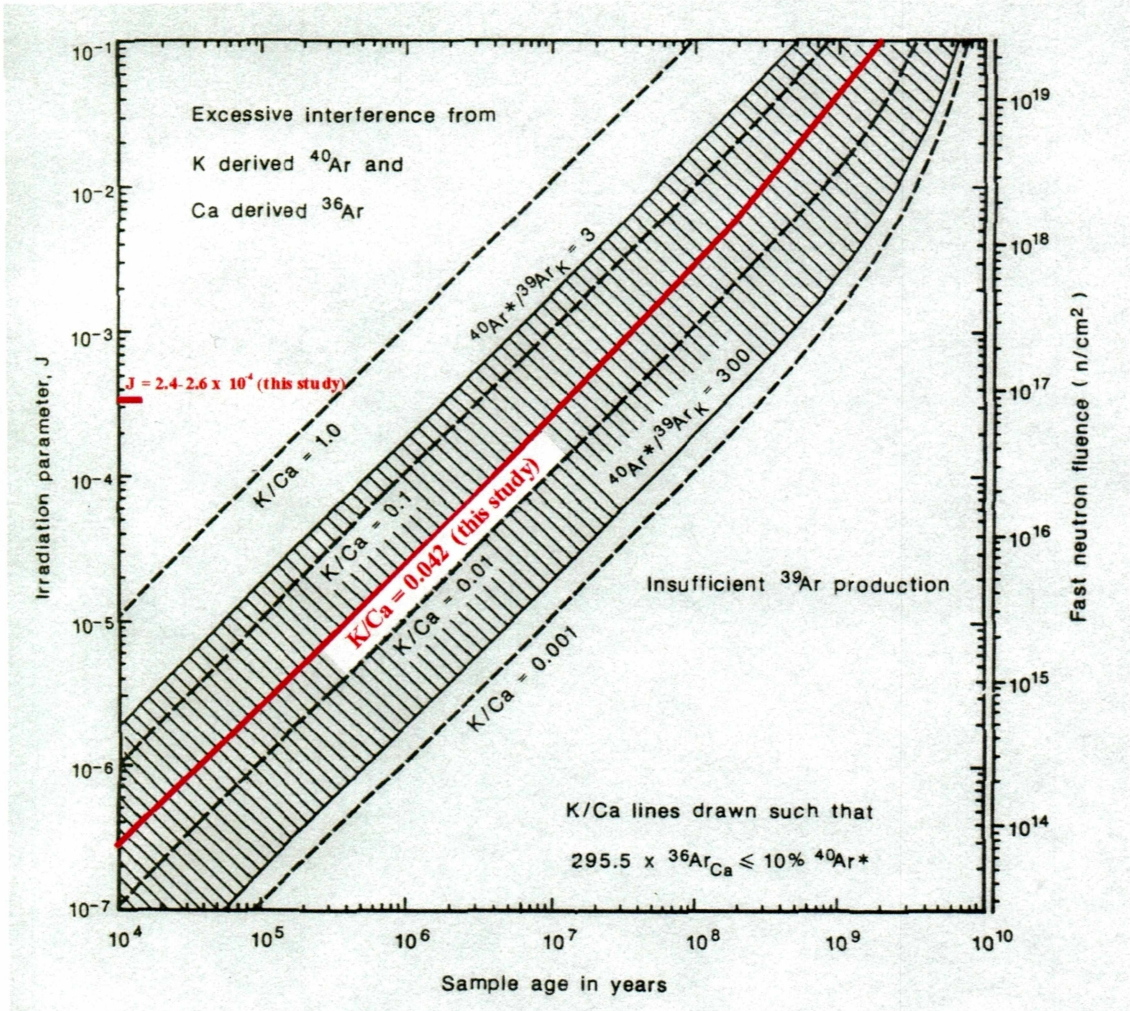

Figure 10: Diagram showing the irradiation parameter, J, required to optimize ^{39}Ar production from ^{39}K for differing age sample while minimizing interference by ^{40}Ar and ^{36}Ar (reproduced from McDougall and Harrison, 1998, p. 59).

Since $^{40}Ar_K$ is produced primarily by slow neutrons (thermal neutrons), this reaction can be avoided by emplacement of a Cd liner around the samples during irradiation. Without $^{40}Ar_K$, the correction factor $(^{40}Ar/^{39}Ar)_K$ becomes zero. One practical problem

associated with this method, however, is the disposal of the radioactive Cd plate. The Cd plate would have been useful in this study, however it was not used.

^{36}Ar produced from the reaction $^{40}Ca(n,n\alpha)^{36}Ar$ interferes with the correction for atmospheric ^{40}Ar by means of the ^{36}Ar found in the sample. The problem of $^{36}Ar_{Ca}$ interference "becomes particularly severe when attempting to date young samples that have low K/Ca ratios" (McDougall and Harrison, 1988, p. 62).

Interference from the $^{42}Ca(n,\alpha)^{39}Ar$ is independent of the fluence and depends only on the K/Ca ratio of the sample. The correction factor $(^{39}Ar/^{37}Ar)_{Ca}$ becomes increasingly important with lower K/Ca ratios.

Another factor to consider during irradiation is the neutron flux gradients. Neutron flux gradients across a reactor must be monitored carefully in order to assign appropriate J (irradiation parameter) values. Conventionally, standards are arranged around the samples during irradiation so that J values can be assigned to samples based on their geometric location relative to the standards. J values are determined for standards based on equation A.3. To approximate more precisely the J value for a sample of young age and low potassium, it may be advantageous to surround the samples with several standards to better determine the geometry of the neutron flux gradient.

Finally, the decay of ^{37}Ar ($t_{1/2}$ = 35.1 +/- 0.1 days, Stoenner and others, 1965) and ^{39}Ar ($t_{1/2}$ = 269 +/- 3 years, Stoenner and others, 1965) since irradiation is an important consideration. Since so little argon isotope is expected in such young, low potassium samples, they must be measured soon after irradiation, and their decay since irradiation must be considered in the final age calculation.

4.3 Parameters Used in this Study

The geochronology lab at the University of Alaska Fairbanks, has two standard target ranges of J values (irradiation time) that are used depending on the expected age of the sample. "Old" samples with much more radiogenic argon are irradiated with a higher J value (longer irradiation time) than "young" samples, such as the hornblende grains in this study. Most of the hornblendes dated in this study were irradiated with a J value of 0.000257 +/- 0.000001. Three earlier runs were irradiated with a J value of 0.000248 +/- 0.000001. Based on the hornblende K/Ca ratio of 0.042 and the calculations represented in Figure 10, it would have been preferable to have had an even shorter irradiation time with a resulting J value in the 10^{-5} to 10^{-6} range. Also, due to problems with the mass spectrometer, the samples were measured longer after their irradiation than would have been preferred. In this case the delay time was 109 days. Even though this delay slightly decreased the amount of ^{37}Ar and ^{39}Ar due to decay, good results were still obtained as will be discussed in the following sections.

4.4 Sample Preparation

Hornblende grains from the bulk tephra were separated in a four-step process. First, the bulk tephra was placed in a sonicator and rinsed several times with deionized water to remove fine material. Second, Sodium Polytungstate (SPT) heavy liquid was used to

separate glass from heavier minerals. The glass and heavy mineral portions were collected separately by vacuum filtration, washed with deionized water then dried in a drying oven at 80°C. Third, the heavy mineral portion, consisting primarily of hornblende, minor pyroxene, minor plagioclase, and magnetite, was sent through a Frantz magnetic separator to extract the bulk of the hornblende from less magnetic mineral phases such as plagioclase and the more magnetic phases such as magnetite. Fourth, since pyroxene and hornblende have the same magnetic susceptibility, the hornblendes were picked out by hand using small tweezers and a binocular scope.

4.5 Total Laser Fusion

Initial $^{40}Ar/^{39}Ar$ dating experiments with the hornblendes in tephra 96TOK1-9 revealed that several grains were needed in order to release enough argon for accurate isotope measurements. For the final age calculation, twenty analyses of total laser fusion of greater than 70 grains of hornblende were performed on the hornblendes from tephra 96TOK1-9. Figure 11 shows each single-step total fusion analysis, in order of youngest to oldest. In general the resulting age of the combined single-fusion analyses seems to be around 700,000 years, but a more sophisticated statistical analysis is needed to determine the age, and to justify which samples to exclude prior to age determination.

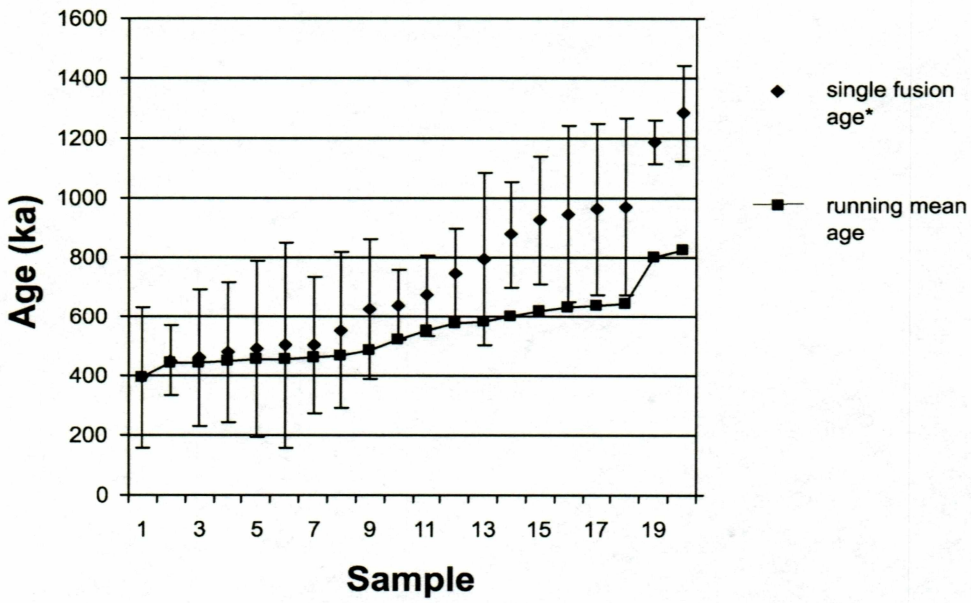

Figure 11: Age of single-step total laser fusion analyses of hornblende from sample 96TOK1-9, arranged from youngest to oldest.

***error bars on each single fusion age indicate one standard deviation**

4.6 Statistical Analysis of Argon Data for Age Determination

Gansecki and others (1998) have established a method to calculate age by utilizing the mean square weighted deviation (MSWD) parameter. This parameter is used to evaluate the source of scatter in the data with a term that weights the error of each run by calculating the square of the inverse of the error. Large error analyses then have less weight in the final calculation then do smaller error analyses.

A MSWD that exceeds the critical value of $(1 + 2[2/(n\text{-}2)]^{1/2})$ for n points indicates a greater than 95% probability that the scatter cannot be explained by analytical error alone and therefore those samples have a justified exclusion from the final age calculation

(Wendt and Carl, 1991). For young tephras such as 96TOK1-9, it is assumed that excess Argon or contamination by older xenocrysts is much more likely to be a problem than Argon loss, thus the running MSWD is calculated by arranging the ages from youngest to oldest (Appendix V). The running MSWD versus the critical MSWD is shown in Figure 13 for the 20 analyses performed on the hornblendes of tephra 96TOK-1-9. To calculate the final age, the four oldest ages are now removed where the running MSWD was greater than the critical MSWD. The resulting age is 627.5 +/- 47.7 ka.

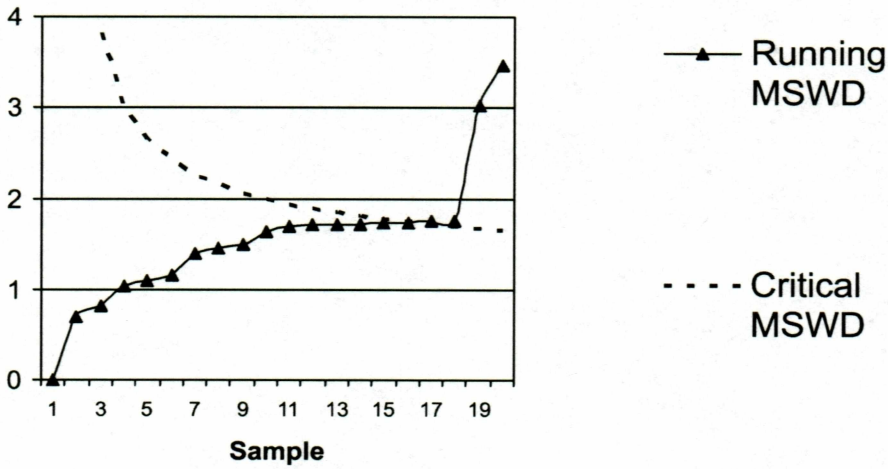

Figure 12: Running MSWD vs. Critical MSWD calculated for each single laser fusion run of multiple grains of hornblende.

Chapter 5: Discussion of Tephra Correlation

5.1 Major Oxide Correlations using the Similarity Coefficient

One way to correlate tephras from different localities is to use a similarity coefficient calculation. A similarity coefficient is calculated by the addition of ratios of each oxide, with each ratio being less than one, then dividing by the total number of ratios added (Borchardt and others, 1972). Similarity coefficients with values of 0.95 or higher are considered to be highly correlative, provided other stratigraphic and geochronologic evidence supports the correlation. For this study, tephras from the Tok section were compared to other tephras in interior Alaska and the Yukon to determine the similarity coefficient (Tables 2 and 3).

Samples 96TOK1-9, 96TOK1-12, and 96TOK1-13, collected in the lower, organic-rich silt unit (Unit 6, Figure 3), have high similarity coefficients (Table 2). Field observations suggest that these tephras are the same. All three are pumiceous, coarse, hornblende-rich, and have the same "salt-and-pepper" appearance. Samples 96TOK1-12 and 96TOK1-13 were taken from isolated pods of tephra approximately 30 cm above sample 96TOK1-9 and likely represent redeposition of the lower, thicker, airfall deposit. Collectively, these samples are here named the "Tetlin Tephra" and their combined geochemistry is listed in Appendix II.

Sample 96TOK1-23 and sample 96TOK1-20 have a similarity coefficient of 0.97. Both were collected in a sandy, micro-pumice layer within a few meters horizontally of

Table 2: Similarity coefficient table for tephras at site 96TOK1 (this study), Gold Hill Loess (Preece and others, 1999), and Dawson Tephra (Westgate and others, 2001). Numbers in bold type indicate a similarity coefficient of 0.96 or greater.

	Site 96TOK1 Tephras									Gold Hill Loess Tephras													
	96TOK1-2	96TOK1-5	96TOK1-9	96TOK1-12	96TOK-1-13	96TOK1-20	96TOK-1-21	96TOK1-22	96TOK-1-23	HH	PA	OC	SC	CF	WP	MF	SP	PH	PT	GI	EAB	LW	DAB	Dawson
96TOK1-2	1.00	0.87	0.87	0.87	0.86	0.88	0.92	0.86	0.88	0.86	0.80	0.89	0.84	0.88	0.83	0.81	0.79	0.76	0.73	0.86	0.83	0.75	0.91	0.88
96TOK1-5		1.00	0.79	0.79	0.78	0.81	0.85	0.76	0.81	0.85	0.74	0.77	0.81	0.82	0.76	0.75	0.73	0.71	0.69	0.91	0.89	0.66	0.91	0.80
96TOK1-9			1.00	**0.99**	**0.98**	**0.96**	0.88	0.87	0.94	0.79	0.81	0.90	0.78	0.91	0.88	0.92	0.91	0.86	0.82	0.79	0.79	0.84	0.82	0.86
96TOK1-12				1.00	**0.99**	**0.96**	0.87	0.87	0.94	0.79	0.81	0.90	0.77	0.91	0.88	0.92	0.91	0.86	0.82	0.79	0.79	0.84	0.82	0.86
96TOK-1-13					1.00	**0.95**	0.86	0.88	0.93	0.78	0.82	0.91	0.76	0.90	0.89	0.92	0.92	0.87	0.83	0.78	0.78	0.85	0.81	0.86
96TOK1-20						1.00	0.90	0.84	**0.97**	0.82	0.78	0.87	0.79	0.95	0.90	0.91	0.89	0.85	0.82	0.80	0.82	0.82	0.83	0.84
96TOK-1-21							1.00	0.81	0.89	0.85	0.75	0.84	0.85	0.94	0.87	0.82	0.83	0.80	0.76	0.83	0.83	0.74	0.87	0.83
96TOK1-22								1.00	0.83	0.78	0.92	**0.96**	0.78	0.79	0.79	0.85	0.82	0.81	0.79	0.81	0.76	0.85	0.83	0.92
96TOK-1-23									1.00	0.81	0.77	0.85	0.78	0.93	0.89	0.92	0.90	0.85	0.82	0.80	0.82	0.80	0.83	0.84
HH										1.00	0.86	0.67	0.76	0.44	0.43	0.35	0.36	0.30	0.26	0.83	0.85	0.67	0.88	0.82
PA											1.00	0.89	0.74	0.74	0.74	0.80	0.77	0.77	0.74	0.79	0.74	0.85	0.81	0.89
OC												1.00	0.78	0.82	0.82	0.87	0.85	0.83	0.80	0.80	0.77	0.83	0.84	0.92
SC													1.00	0.58	0.56	0.46	0.48	0.40	0.35	0.77	0.76	0.66	0.81	0.79
CF														1.00	0.92	0.87	0.88	0.84	0.80	0.80	0.80	0.78	0.84	0.80
WP															1.00	0.87	0.91	0.84	0.80	0.76	0.76	0.78	0.79	0.77
MF																1.00	0.94	0.93	0.89	0.74	0.76	0.82	0.76	0.82
SP																	1.00	0.91	0.86	0.73	0.77	0.79	0.75	0.80
PH																		1.00	0.94	0.70	0.74	0.82	0.72	0.81
PT																			1.00	0.68	0.71	0.84	0.70	0.77
GI																				1.00	0.88	0.71	0.93	0.84
EAB																					1.00	0.65	0.86	0.79
LW																						1.00	0.72	0.81
DAB																							1.00	0.87
Dawson																								1.00

Table 3: Similarity coefficient table for tephras at site 96TOK1 (this study) and tephras in the Klondike district of the Yukon (Preece and others, 2000). Numbers in bold type indicate a similarity coefficient of 0.96 or greater.

	96TOK1-2	96TOK1-5	96TOK1-9	96TOK1-12	96TOK-1-13	96TOK1-20	96TOK-1-21	96TOK1-22	96TOK-1-23	Dawson	Old Crow	Mosquito Gulch	Dominion Creek	Bonanza Creek	Sheep Creek	80 Pup	Preido Hill	Last Chance Creek	Little Blanche Creek	Quartz Creek
96TOK1-2	1.00	0.87	0.87	0.87	0.86	0.88	0.92	0.86	0.88	0.87	0.88	0.82	0.76	0.73	0.89	0.92	0.82	0.86	0.83	0.73
96TOK1-5		1.00	0.79	0.79	0.78	0.81	0.85	0.76	0.81	0.80	0.76	0.75	0.67	0.83	0.85	0.87	0.77	0.78	0.76	0.66
96TOK1-9			1.00	**0.99**	**0.98**	**0.96**	0.88	0.87	0.94	0.86	0.89	0.81	0.84	0.66	0.85	0.87	0.88	**0.96**	0.95	0.80
96TOK1-12				1.00	**0.99**	**0.96**	0.87	0.87	0.94	0.86	0.89	0.81	0.84	0.66	0.85	0.86	0.89	0.94	**0.96**	0.81
96TOK-1-13					1.00	0.95	0.86	0.88	0.93	0.86	0.90	0.80	0.85	0.65	0.84	0.85	0.88	0.95	**0.96**	0.82
96TOK1-20						1.00	0.90	0.84	**0.97**	0.83	0.85	0.79	0.81	0.68	0.88	0.89	0.89	0.94	0.94	0.78
96TOK-1-21							1.00	0.81	0.89	0.82	0.83	0.81	0.76	0.74	**0.96**	0.93	0.87	0.90	0.86	0.71
96TOK1-22								1.00	0.83	0.91	**0.98**	0.84	0.86	0.64	0.79	0.86	0.80	0.87	0.87	0.83
96TOK-1-23									1.00	0.83	0.84	0.79	0.79	0.68	0.87	0.88	0.92	0.92	0.94	0.79
Dawson										1.00	0.91	0.86	0.83	0.68	0.80	0.87	0.82	0.84	0.83	0.80
Old Crow											1.00	0.84	0.86	0.65	0.80	0.86	0.81	0.89	0.88	0.82
Mosquito Gulch												1.00	0.75	0.75	0.80	0.83	0.81	0.83	0.80	0.71
Dominion Creek													1.00	0.57	0.75	0.75	0.77	0.84	0.84	0.88
Bonanza Creek														1.00	0.76	0.74	0.67	0.67	0.65	0.55
Sheep Creek															1.00	0.91	0.84	0.87	0.84	0.70
80 Pup																1.00	0.83	0.88	0.85	0.71
Preido Hill																	1.00	0.87	0.89	0.83
Last Chance Creek																		1.00	0.95	0.79
Little Blanche Creek																			1.00	0.82
Quartz Creek																				1.00

each other in the loess of Unit 5, so the high similarity coefficient was expected. Two of the more significant correlations that appear in the similarity coefficient calculation are the similarity of sample 96TOK1-22 and the Old Crow Tephra (0.96, Table 2) and the similarity of sample 96TOK1-21 and the Sheep Creek Tephra (0.96, Table 3). This similarity is further illustrated in the oxide variation diagrams of SiO_2 vs. Al_2O3, CaO, and Na_2O (Figure 13). Sample 96TOK1-21 clearly falls within the range of Sheep Creek Tephra samples collected in Alaska and the Yukon and sample 96TOK1-22 falls in the range of the Old Crow Tephra samples. Sample 96TOK1-22 occurs in the loess of unit 5, as a discontinuous, 1- to 5-cm thick deposit of fine white ash, approximately 0.5 meters above 96TOK1-21. Both the Old Crow Tephra and sample 96TOK1-22 are composed of platey, tricuspate bubble-wall shards (Figure 5). Their glass morphology and major oxide chemistry indicate that these two tephras are both type I. Sample 96TOK1-21 and the Sheep Creek Tephra are both type II tephras and consist of highly inflated pumice. The Old Crow Tephra and the Sheep Creek Tephra are important marker beds in Alaska and the Yukon; their correlation over diverse late Pleistocene sediments has greatly advanced the understanding of the late Pleistocene geologic history of the area (Westgate and others, 2001). This correlation of tephra 96TOK1-22 with the Old Crow Tephra and 96TOK1-21 with the Sheep Creek Tephra, combined with the stratigraphic descriptions of the bracketing silt and sands will provide researchers with additional critical information to piece together the late Pleistocene history of this part of interior Alaska.

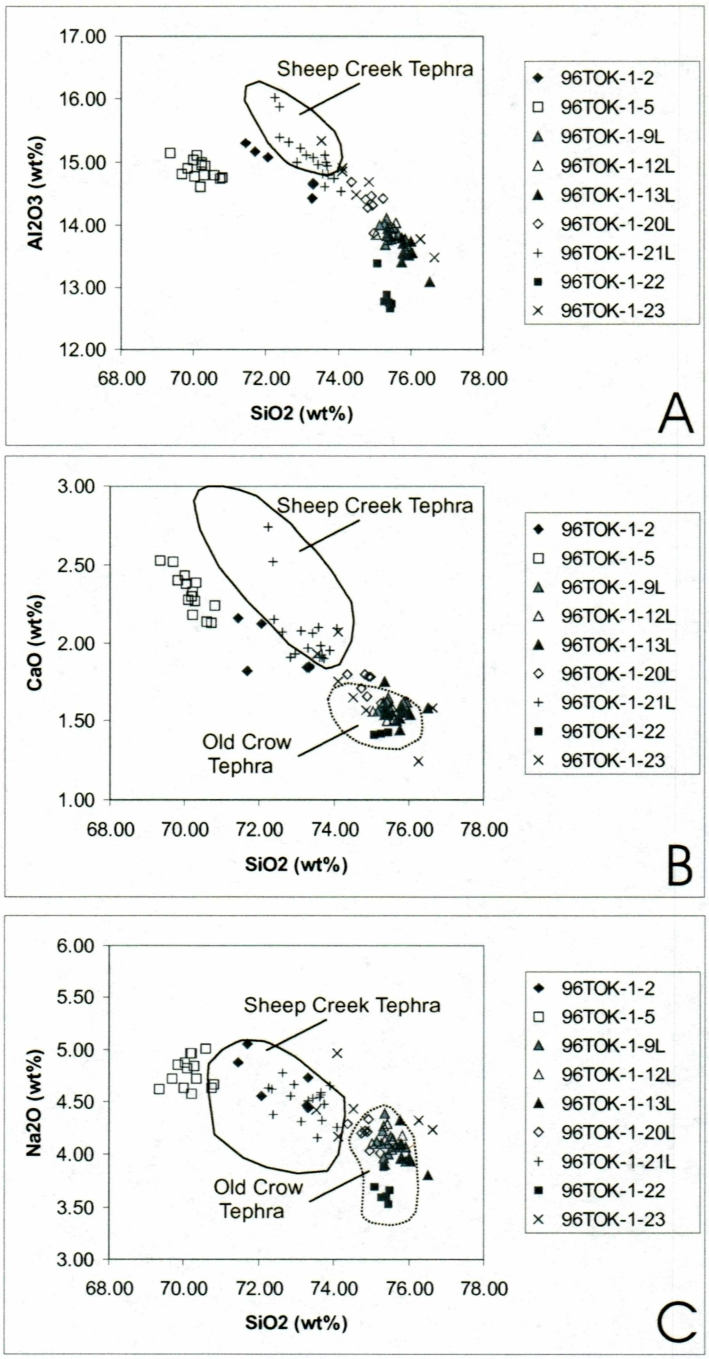

Figure 13: Oxide variation diagrams showing the range of glass compositions of Sheep Creek Tephra (Preece and others, 1999; Preece and others, 2000) and Old Crow Tephra (Preece and others, 2000) compared to tephras at site 96TOK1.

5.2 Discussion of Age Control

Three tephras in the Tok section provide stratigraphic age control: samples 96TOK1-9 (Tetlin Tephra), 96TOK1-21, and 96TOK1-22 (Figure 14). Tephra sample 96TOK-1-9 (Tetlin Tephra), in the lower part of the section has an age of 627.5 +/- 47.7 ka ($^{40}Ar/^{39}Ar$ age of hornblende, this study). Unfortunately, this tephra does not correlate definitively with any tephras that have been dated in interior Alaska or the Yukon, so there is no independent age control and therefore it is important to make sure that this age makes sense stratigraphically. Based on glass morphology and major oxide chemistry, tephra sample 96TOK1-22 is correlated with the Old Crow Tephra and tephra sample 96TOK1-21 is correlated with the Sheep Creek Tephra. The Old Crow Tephra has been dated by the Isothermal Plateau Fission Track (ITPFT) method at 140 +/- 10 ka (Westgate and others, 1990; Preece and others, 1999) and the Sheep Creek Tephra has been dated from thermoluminescence of bracketing loess at 190 +/- 20 ka (Berger and others, 1996). This makes sense stratigraphically since tephra sample 96TOK1-22 occurs approximately 0.5 meters above tephra 96TOK1-21 and tephra 96TOK1-21 occurs about 1 meter above the older, 627 ka tephra 96TOK1-9. The age relationships and correlations are summarized in Figure 14.

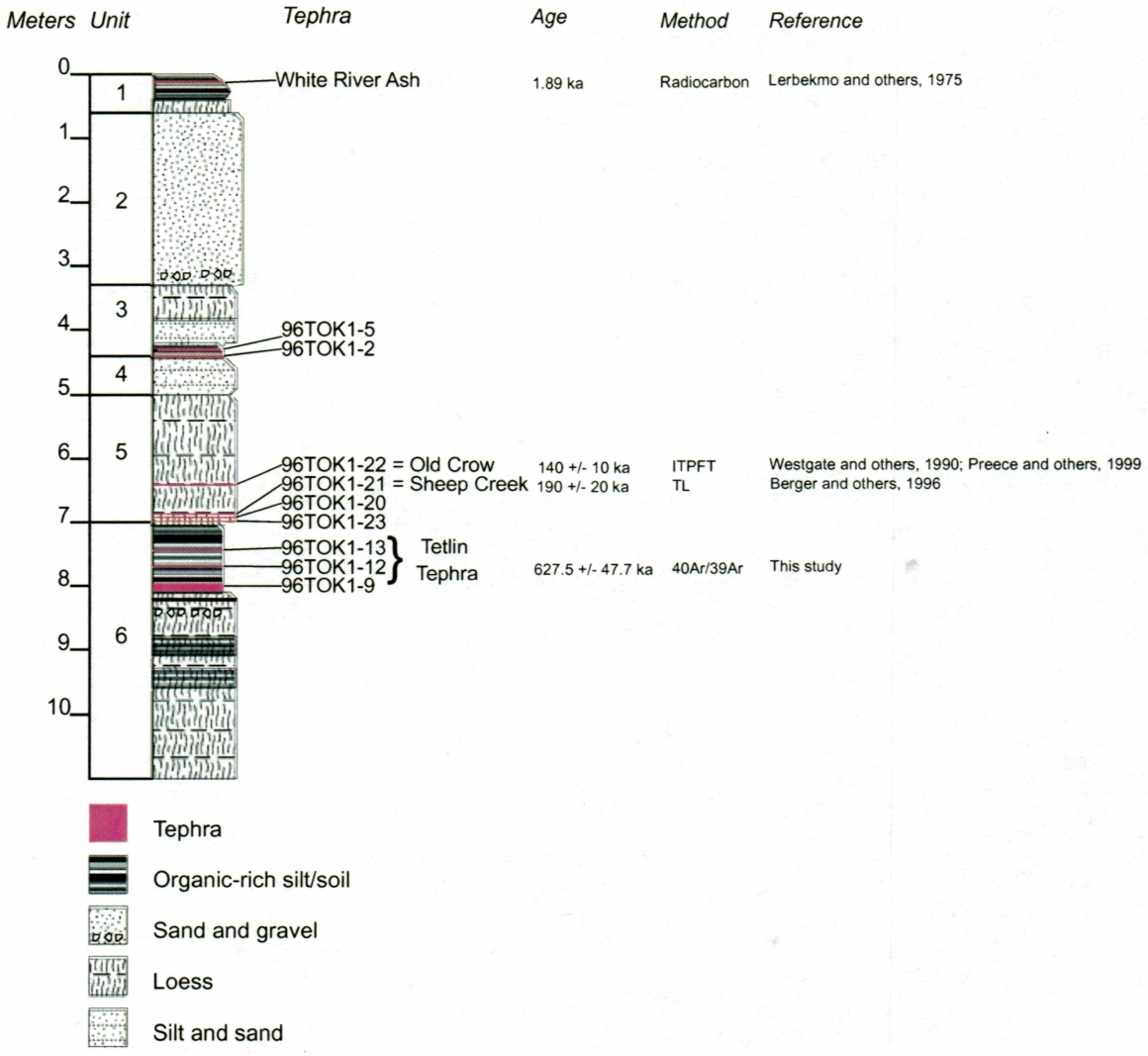

Figure 14: Summary stratigraphic section showing age relationships and tephra correlations.

5.3 Lithostratigraphic Interpretation

The combination of lithologic unit descriptions with the age constraints that are based on the tephra correlations and the $^{40}Ar/^{39}Ar$ dating completed for this study, results

in a lithostratigraphic interpretation of site 96TOK1 that is summarized in Figure 15. Stratigraphic unit 1 corresponds to the Holocene interglacial period, oxygen isotope stage 1 (OIS 1), with the development of soils and loess. Units 2 and 3 correspond to OIS 2 and OIS 3, and represent the Wisconsinan glacial period with the accumulation of sand, gravel, and silt. Unit 4 (OIS 4) is likely the early Wisconsinan onset of silt and gravel accumulation. Unit 5 corresponds to the last interglacial (OIS 5) and into OIS 6 and 7 and contains abundant loess. The Old Crow Tephra and the Sheep Creek Tephra are at the base of this unit. A large unconformity is observed at the base of unit 5, where over 300,000 years are missing from the section. Below unit 5, unit 6 contains soil, loess, and ash. The Tetlin Tephra near the top of unit 6 was dated at 627.7 +/- 47.5 ka, making this section middle to early Pleistocene in age.

5.4 Discussion of Source Vent Candidates

The proximity of the tephra site described in this study to the Wrangell volcanic field makes the Wrangells an obvious choice to consider as the source area for many of these tephras. The tephras collected for this study are located only about 100 miles north of the Wrangell volcanic field and consist primarily of type II tephras, with the two exceptions being 96TOK-1-22 (correlated to Old Crow Tephra, a type I tephra) and 96TOK-1-5. Previous investigations by Westgate and others (1994), Preece (1997), and Preece and others (1999) have linked type II tephras to Mount Drum and Mount

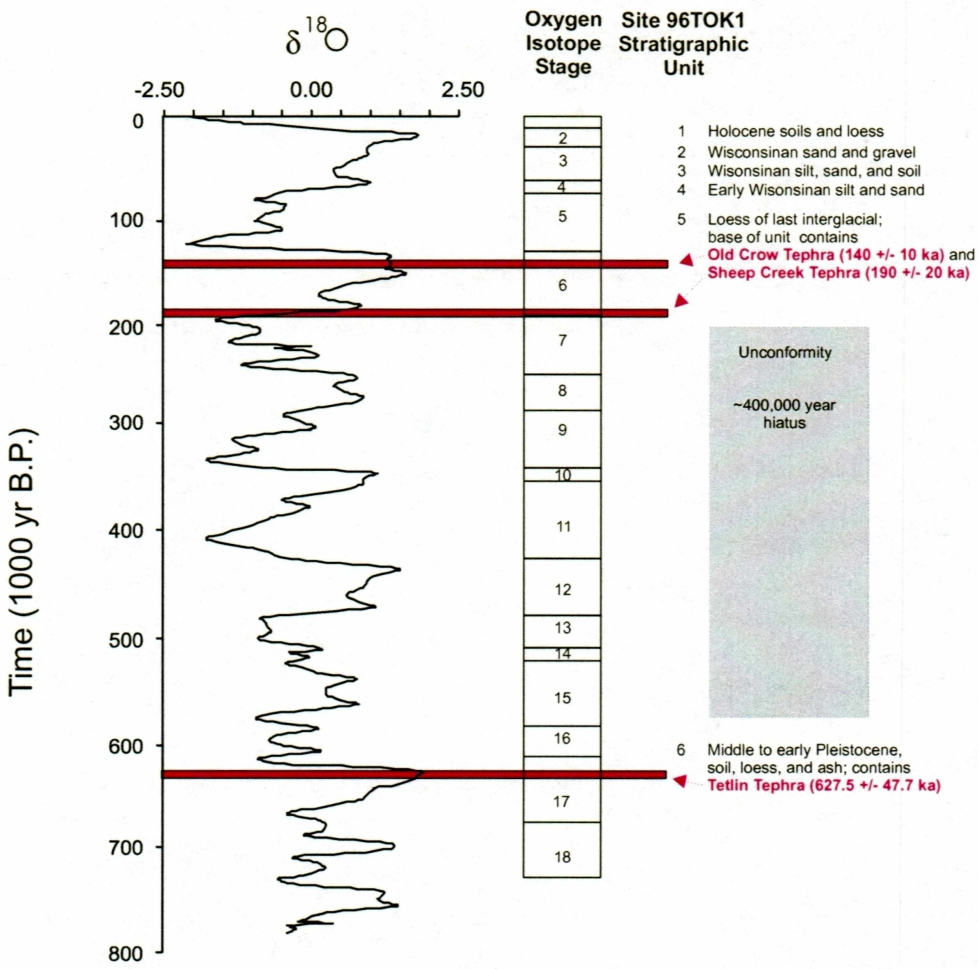

Figure 15: Lithostratigraphic interpretation of site 96TOK1. Oxygen isotopic variations and timescale from Imbrie and others, 1984; Oxygen isotope stage boundaries from Hays and others, 1976, Kominz and others, 1979, and Pisias and Moore, 1981.

Churchill in the Wrangell volcanic field, and at Hayes volcano in the northeastern part of the Alaska Peninsula. Mount Drum and Mount Churchill are the only two Wrangell area volcanoes with documented silicic explosive activity. The proximity of the Wrangells to

the predominantly type II tephra section described here supports the idea that the Wrangell volcanic field is the source of type II tephras.

The thickness of the Tetlin Tephra indicates its deposition was the result of a large explosive eruption. Its composition (highly inflated pumice with abundant euhedral hornblende) matches that of the hornblende dacites described on Mount Drum (Richter and others, 1994). The results of $^{40}Ar/^{39}Ar$ dating indicate that the deposition of the Tetlin Tephra occurred approximately 627 ka. Based on published geologic descriptions and geochemistry of the Wrangell volcanic field, the most likely candidates for proximal correlation are the 650 to 400 ka silicic domes that are found on the east and southeast flank of Mount Drum volcano.

Based on age and composition, the 650 to 400 ka eruptive sequence of Mount Drum is the most likely source for the 627-ka Tetlin Tephra. Between 650 and 400 ka, a group of four silicic domes were emplaced on the east and southeast flank of the volcano (K-Ar whole rock ages by Richter and others, 1994). These rhyodacite domes are porphyritic, consisting of brown hornblende, plagioclase, and rare to common hypersthene, biotite, and augite, much like the composition of Tetlin Tephra. All rocks analyzed from Mount Drum have type II rare earth element characteristics: they are LREE-enriched, having La/Yb between 9 to 25 (Richter and others, 1994). No other Wrangell source vents have documented eruptive products or the right age constraints to match the age and composition of the Tetlin Tephra other than the Mount Drum domes. The Tetlin Tephra

likely represents an early explosive phase of activity associated with the emplacement of these 650 to 400 ka, petrologically similar domes.

Chapter 6: Summary and Conclusions

This thesis documents a Pleistocene tephra section near Tok, Alaska. The most significant findings of this study are 1) the determination of the age of 627.5 +/- 47.7 ka for the newly named Tetlin Tephra (sample 96TOK1-9) by a process of several runs of single-step total laser fusion of multiple grains of low K hornblende, 2) the correlation of the 140 +/- 10 ka Old Crow Tephra to tephra 96TOK1-22 found in the stratigraphic section described in this study, 3) the correlation of the 190 +/- 20 ka Sheep Creek Tephra to tephra 96TOK1-21 found in the stratigraphic section described in this study, and 4) the documentation of several type II tephras in the vicinity of the Wrangell volcanic field, and the documentation of one type II tephra that has the same age and composition as proximal deposits on Mount Drum. This further supports the idea of the Wrangell volcanic field as the source of type II tephras found in interior Alaska and the Yukon. Table 4 summarizes the type II tephra occurrences in Alaska and the Yukon Territory with the addition of the results from this study.

The ability to date young, low K hornblende such as the hornblendes dated in this study will be encouraging to other researchers hoping to find a method for age determination for similar samples. It has been shown that with the use of single-step laser fusion and multiple runs, a well-constrained age can be obtained. The amount of sample is critical in that it takes several grains and multiple runs to apply the statistics of Gansecki and others (1998) and Wendt and Carl (1991) to arrive at a meaningful age.

Table 4: Summary of ages of distal type II tephra bed occurrences in Alaska and the Yukon Territory (modified from Preece, 1997, with new data from this study).

Tephra	Age	Age Reference	Location
East White River Ash	1147 BP	Clague and others, 1995.	Alaska and Yukon
North White River Ash	1890 BP	Lerbekmo and others, 1975	Alaska and Yukon
Surprise Creek Tephra	0.18 Ma	Westgate and others, 1995	Old Crow Basin, YK
Sheep Creek Tephra	0.19 Ma	Berger and others, 1996	Alaska and Yukon
Tetlin Tephra	**0.63 Ma**	**This study**	**Tetlin Junction, Alaska**
PH Tephra	Between 0.6 and 0.78 Ma	Westgate, unpublished data	Fairbanks, Alaska
SP Tephra	0.87 Ma	Preece and others, 1999	Fairbanks, Alaska
WP Tephra	1.03 Ma	Westgate and others, 1990	Fairbanks, Alaska
Fort Selkirk	1.49 Ma	Westgate and others, 1990	Fort Selkirk, YK
Little Timber	2.29 Ma	Westgate and others, 1995	Old Crow Basin, YK

The correlation of 96TOK1-22 at this site with the widespread Old Crow Tephra, and the correlation of 96TOK1-21 at this site with the Sheep Creek Tephra, combined with the stratigraphic descriptions of the bracketing silt and sands provide valuable information for interpretation of the late Pleistocene history of this part of interior Alaska. Sites such as the tephra section described in this study are unusual and highly valued. They provide a critical time-stratigraphic framework for the related fields of climate study, palynology, and glacial history.

The eruptive history of the Wrangell volcanic field has not been well-documented, so the discovery and geochemical characterization of tephras in the vicinity is an important step towards the understanding of the eruptive history of these vents. Of particular interest is the apparent large explosive eruption that accompanied the dome building phase at Mount Drum 627 thousand years ago. As tephrochronologists and Quaternary researches discover more tephra/loess sections in the interior of Alaska and the Yukon, more type II tephras will likely be documented and correlated to the tephras described at this site, thus further defining the eruptive history of this volcano.

References

Becker, T.A., Sharp, W.D., Renne, P.R., Turrin, B.D., Page, W.D., Wakabayashi, J., 1994, $^{40}Ar/^{39}Ar$ dating of young low-K tholeiites: examples from northeast California, U.S.A., *In* Abstracts of the eighth international conference on geochronology, cosmochronology, and isotope geology: U. S. Geological Survey Circular, p. 24.

Berger, G.W., Péwé, T. L., Westgate, J.A., Preece, S.J., 1996, Age of the Sheep Creek tephra (Pleistocene) in central Alaska from thermoluminescence dating of bracketing loess: Quaternary Research, v. 45, p. 263-270.

Berger, G.W., Pillans, B.J., Palmer, A.S., 1992, Dating loess up to 800 ka by thermoluminescence: Geology, v. 20, no. 5, p. 403-406.

Borchardt, G.A., Aruscavaga, P.J., Millard, H.T., Jr., 1972, Correlation of the Bishop Ash, a Pleistocene marker bed, using instrumental neutron activation analysis: Journal of Sedimentary Petrology v. 42, p. 301-306.

Clague, J.J., Evans, S.G., Rampton, V.N., Woodsworth, G.J., 1995, Improved age estimates for the White River and Bridge River tephras, western Canada: Canadian Journal of Earth Sciences, v. 32: 1,172-1,179.

Gansecki, C.A., Mahood, G.A., McWilliams, M., 1998, New ages for the climatic eruptions at Yellowstone: Single-crystal $^{40}Ar/^{39}Ar$ dating identifies contamination: Geology, v. 26, no. 4, p. 343-346.

Hays, J.D., Imbrie, J., and Shackleton, N.J., 1976, Variations in the earth's orbit: pacemaker of the ice ages: Science, v. 194, p. 1121-1132.

Hays, J.D., Kukla, G., and Saltzman, B., 1984, Milankovitch and Climate, Part 1: NATO ASI Series C: Mathematical and Physical Sciences, v. 126, p. 269-305.

Hildreth, W., 1983, The compositionally zoned eruption of 1912 in the Valley of Ten Thousand Smokes, Katmai National Park, Alaska: Journal of Volcanology and Geothermal Research, v. 18, no. 1-4, p. 1-56.

Hu, Q., Smith, P.E., Evenson, N.M., York, D., 1994, Lasing in the Holocene: extending the $^{40}Ar/^{39}Ar$ laser probe method into the 14C age range: Earth and Planetary Science Letters, vol. 123, p. 331-336.

Imbrie, J., Hays, J.D., Martinson, D.G., McIntyre, A., Mix, A.C., Morley, J.J., Pisias, N.G., Prell, W.L., and Shackleton, N.J., 1984, The orbital theory of Pleistocene climate: support from a revised chronology of the marine $\delta^{18}O$ record *in* Berger, A., Imbrie, J.,

Kominz, M.A., Heath, G.R., Ku, T-L., and Pisias, N.G., 1979, Brunhes time scales and the interpretation of climatic change: Earth and Planetary Science Letters, v. 45, p. 394-410.

Layer, P.W., Hall, C.M., York, D., 1987, The derivation of $^{40}Ar/^{39}Ar$ spectra of single grains of hornblende and biotite by laser step-heating: Geophysical Research Letters, v. 14, no. 7, p. 757-760.

Lerbekmo, J.F., Westgate, J.A., Smith, D.G., and Denton, G.H., 1975, New data on the character and history of the White River volcanic eruption, Alaska: in Suggate, R.P., and Cresswell, M.M: Quaternary Studies. Wellington, The Royal Society of New Zealand, p. 203-209.

Lowe, P.C, Richter, D.H., Smith, R.L, Schmoss, H.R., 1982, Geologic map of the Nabesna B-5 quadrangle, Alaska: U.S. Geological Survey Geologic Quadrangle Map GQ-1566, 1 sheet, scale 1:63,360.

McDougall, I., and Harrison, T.M., 1988, Geochronology and Thermochronology by the $^{40}Ar/^{39}Ar$ Method: Oxford University Press, ISBN0-19-504302-2, 212 p.

Nye, C.J, 1983, Petrology and geochemistry of Okmok and Wrangell volcanoes, Alaska: Ph.D. dissertation, University of California, Santa Cruz, 205 p.

Péwé, T.L, 1975, Quaternary geology of Alaska: U.S. Geological Survey Professional Paper 835, 145 p.

Pisias, N.G., and Moore, T.C., 1981, The evolution of Plesitocene climate: a time series approach: Earth and Planetary Science Letters, v. 52, p. 450-458.

Preece, S.J., Westgate, J.A., Alloway, B.V., and Milner, M.W., 2000, Characterization, identity, distribution, and source of late Cenozoic tephra beds in the Klondike district of the Yukon, Canada: Canadian Journal of Earth Science, v. 37, p. 983-996.

Preece, S.J., Westgate, J.A., Stemper, B.A., Péwé, T.L., 1999, Tephrochronology of late Cenozoic loess at Fairbanks, central Alaska: GSA Bulletin, v. 111, p. 71-90.

Preece, S.J., 1997, Geochemical variation in the <5 Ma Wrangell volcanic field, Alaska, with an emphasis on the Skookum Creek Volcanic Comples: Ph.D. dissertation, Miami University, 548 p.

Preece, S.J., 1991, Tephrostratigraphy of the late Cenozoic Gold Hill Loess, Fairbanks Area, Alaska, M.S. Thesis, University of Toronto, 164 p.

Preece, S.J., Westgate, J.A., Gorton, M.P., 1992, Compositional Variation and Provenance of Late Cenozoic Distal Tephra Beds, Fairbanks Area, Alaska: Quaternary International, vol. 13/14, p. 97-101.

Richter, D.H., Moll-Stalcup, E.J., Miller, T.P., Lanphere, M.A., Dalrymple, G.B., Smith, R.L., 1994, Eruptive history and petrology of Mount Drum volcano, Wrangell Mountains, Alaska: Bulletin of Volcanology, v. 56, p. 29-46.

Richter, D.H., Ratte, J.C., Schmoll, H.R., Leeman, W.P., Smith, J.G., Yehle, L.A., 1989, Geologic map of the Gulkana B-1 quadrangle, Alaska: U.S. Geological Survey Geologic Quadrangle Map GQ-1655, 1 sheet, scale 1:63,360.

Richter, D.H., Schmoll, H.R., Bove, D.J., 1988, Source of the Sanford volcanic debris flow, south-central Alaska: U.S. Geological Survey Circular 1016, p. 114-116.

Richter, D.H. and Smith, R.L., 1976, Geologic map of the Nabesna A-5 quadrangle, Alaska: U.S. Geological Survey Geologic Quadrangle Map GQ-1292, 1 sheet, scale 1:63,360.

Richter, D.H., Smith, J.G., Lanphere, M.A., Dalrymple, G.B., Reed, B.L., and Shew, Nora, 1990, Age and progression of volcanism, Wrangell volcanic field, Alaska: Bulletin of Volcanology, v. 53, p. 29-44.

Richter, D.H., Smith, R.L., Yehle, L.A., Miller, T.P., 1979, Geologic map of the Gulkana A-2 quadrangle, Alaska: U.S. Geological Survey Quad Map GQ-1520, 1 sheet, scale 1:63,360.

Stoenner, R.W., Schaeffer, O.A., and Katcoff, S., 1965, Half-lives of argon-37, argon-39, and argon-42: Science, vol. 148, p. 1325-1328.

Wendt, I. and Carl, C., 1991, The statistical distribution of the mean square weighted deviation: Chemical Geology, v. 86, p. 275-285.

Westgate, J.A., Preece, S.J., Froese, D.G., Walter, R.C., Sandhu, A.S., and Schweger, C.E., 2001, Dating early and middle Pleistocene glaciations in central Yukon by tephrochronology: Quaternary Research, no. 56, p. 335-348.

Westgate, J.A., Schweger, C., Sandhu, A., Morlan, R., and Matthews, J., 1995, Tephrochronological, paleomagnetic and paleoenvironmental studies of late Cenozoic deposits in the northern Yukon, Canada. 1995 INQUA meeting in Berlin.

Westgate, J.A., Stemper, B.A., and Péwé, T.L., 1990, A 3 m.y. record of Pliocene-Pleistocene loess in interior Alaska. Geology v. 18, p. 858-861.

Westgate, J.A., Perkins, W.T., Fuge, R., Pearce, N.J.G., and Wintle, A.G., 1994, Trace-element analysis of volcanic glass shards by laser ablation inductively coupled plasma mass spectrometry: application to tephrochronological studies: Applied Geochemistry, v. 9, p. 323-335.

Westgate, J.A., Walter, R.C., Pearce, G.W., and Gorton, M.P., 1985, Distribution, stratigraphy, petrochemistry, and paleomagnetism of the late Pleistocene Old Crow tephra in Alaska and the Yukon: Canadian Journal of Earth Sciences 22, p. 893-906.

Williams, K.L., 1987, An introduction to X-ray spectrometry, X-ray fluorescence and electron microprobe analysis: Allen & Unwin, Inc., ISBN 0-04-544001-8, 370 p.

York, D., Hall, C.M., Yanase, Y., Hanes, J.A., Kenyon, W.J., 1981, $^{40}Ar/^{39}Ar$ dating of terrestrial minerals with a continuous laser: Geophysical Research Letters, v. 8, no. 11, p. 1136-1138.

Appendix I: Electron Microprobe Calibration Standards and Detection Limits

Calibration Standards

Parenthesis following element indicate for what analysis these standard were used for; plagioclase = pl, hornblende = hbl, glass = gl.

Element	Standard	Source
Na (pl and hbl)	TALBITE	-
Na (gl)	CCNM	Smithsonian
Al (pl)	TALBITE	-
Al (hbl)	OR10	Taylor
Al (gl)	CCNM	Smithsonian
Si (pl)	TALBITE	-
Si (hbl)	OR10	Taylor
Si (gl)	CCNM	Smithsonian
K (pl and hbl)	OR10	Taylor
K (gl)	CCNM	Smithsonian
Ca (pl)	ANTHITE	Smithsonian
Ca (hbl)	SPHENE1A	Taylor
Ca (gl)	BGLASS3	Smithsonian
Fe (pl)	OR10	Taylor
Fe (hbl)	SALM	-
Fe (gl)	BGLASS3	Smithsonian
F (hbl)	CAF2	Taylor
Mg (pl and hbl)	SPIN	Taylor
Mg (gl)	BGLASS3	Smithsonian
Cl (hbl)	SPGA	Taylor
Cl (gl)	SCAP	Smithsonian
Ti (hbl)	SPHENE1A	Taylor
Ti (gl)	BGLASS2	Smithsonian
Mn (hbl)	WILL	Taylor

3 Sigma Statistical Lower Limit of Detection (LLD) from Williams (1987)

LLD = (6/m)*(Cb/Tb)^0.5

m = sensitivity = counts/sec on the element in the standard divided by the wt.% of the element in the standard

Cb = background counts/sec

Tb = 2*tb

tb = background counting time in seconds

Element	Standard	tb	Tb	Peak (c/s)	Bkg (c/s)	wt.%	m	LLD wt.%
K	OR10	10	20	804.89	4.7	13.43	59.932241	0.05
Ca	SPHENE1A	10	20	1640.87	10.9	20.57	79.770053	0.06

Appendix II. Glass Shard Major Oxide Geochemistry

All results are presented as wt.% oxide except Cl. Iron is reported as Fe_2O_3. Analyses are normalized to 100%. An "L" following the sample name indicates that a "light" fraction of the sample was analyzed, i.e., heavy minerals were removed before microprobe analysis.

Sample: 96TOK-1-2
April 1997

	Na20	MgO	Al203	Si02	Cl	K20	CaO	Ti02	Fe203	Total
96TOK-1-2	4.44	0.43	14.67	73.32	0.33	3.24	1.85	0.05	1.69	100.00
96TOK-1-2	4.73	0.39	14.64	73.32	0.32	2.95	1.84	0.08	1.73	100.00
96TOK-1-2	4.47	0.36	14.43	73.28	0.30	3.52	1.84	0.11	1.69	100.00
96TOK-1-2	4.56	0.46	15.08	72.06	0.35	3.28	2.12	0.25	1.84	100.00
96TOK-1-2	5.05	0.39	15.17	71.69	0.34	3.46	1.82	0.35	1.74	100.00
96TOK-1-2	4.87	0.42	15.30	71.44	0.40	3.50	2.16	0.22	1.71	100.00
AVG	**4.69**	**0.41**	**14.88**	**72.52**	**0.34**	**3.33**	**1.94**	**0.18**	**1.73**	**100.00**
STDDEV	**0.22**	**0.03**	**0.32**	**0.81**	**0.03**	**0.20**	**0.14**	**0.11**	**0.05**	**0.00**
n=6										

Sample: 96TOK-1-5
April 1997

	Na20	MgO	Al203	Si02	Cl	K20	CaO	Ti02	Fe203	Total
96TOK-1-5	4.67	0.64	14.76	70.81	0.20	3.07	2.24	0.56	3.06	100.00
96TOK-1-5	4.63	0.73	14.74	70.72	0.15	3.18	2.13	0.52	3.21	100.00
96TOK-1-5	5.01	0.66	14.80	70.58	0.19	3.06	2.14	0.58	2.98	100.00
96TOK-1-5	4.72	0.82	14.95	70.32	0.10	2.84	2.39	0.60	3.25	100.00
96TOK-1-5	4.84	0.73	14.79	70.27	0.16	2.98	2.27	0.62	3.34	100.00
96TOK-1-5	4.58	0.71	15.00	70.22	0.14	3.04	2.33	0.58	3.40	100.00
96TOK-1-5	4.96	0.73	14.96	70.22	0.17	3.02	2.18	0.75	3.00	100.00
96TOK-1-5	4.96	0.77	14.62	70.18	0.15	2.79	2.30	0.59	3.64	100.00
96TOK-1-5	4.82	0.75	15.12	70.09	0.17	2.98	2.28	0.53	3.25	100.00
96TOK-1-5	4.88	0.76	14.78	70.01	0.20	2.96	2.38	0.81	3.21	100.00
96TOK-1-5	4.63	0.65	15.03	69.98	0.15	2.95	2.43	0.81	3.38	100.00
96TOK-1-5	4.85	0.76	14.90	69.82	0.21	3.20	2.40	0.40	3.46	100.00
96TOK-1-5	4.72	0.81	14.82	69.68	0.21	3.10	2.52	0.66	3.48	100.00
96TOK-1-5	4.62	0.89	15.14	69.35	0.14	2.93	2.53	0.87	3.52	100.00
AVG	**4.78**	**0.74**	**14.89**	**70.16**	**0.17**	**3.01**	**2.32**	**0.63**	**3.30**	**100.00**
STDDEV	**0.14**	**0.07**	**0.15**	**0.38**	**0.03**	**0.11**	**0.12**	**0.13**	**0.19**	**0.00**
n=16										

Appendix II: continued

Sample: 96TOK-1-9L
December 1996

	Na20	MgO	Al203	Si02	Cl	K20	CaO	Ti02	Fe203	Total
96TOK-I-9L	4.07	0.32	13.52	75.93	0.03	3.13	1.62	0.21	1.17	100.00
96TOK-I-9L	3.94	0.34	13.66	75.91	0.04	3.12	1.59	0.21	1.18	100.00
96TOK-I-9L	3.96	0.34	13.78	75.84	0.10	2.81	1.62	0.21	1.34	100.00
96TOK-I-9L	4.07	0.35	13.86	75.65	0.03	3.15	1.50	0.23	1.14	100.00
96TOK-I-9L	4.17	0.33	13.96	75.51	0.02	3.20	1.57	0.19	1.04	100.00
96TOK-I-9L	4.00	0.32	13.77	75.46	0.05	3.24	1.65	0.15	1.36	100.00
96TOK-I-9L	4.10	0.39	13.81	75.42	0.05	3.15	1.63	0.21	1.23	100.00
96TOK-I-9L	4.39	0.42	13.83	75.36	0.04	2.97	1.60	0.08	1.31	100.00
96TOK-I-9L	3.97	0.39	14.12	75.34	0.04	3.19	1.58	0.22	1.15	100.00
96TOK-I-9L	4.22	0.31	13.69	75.31	0.05	3.06	1.61	0.49	1.27	100.00
96TOK-I-9L	4.10	0.39	14.01	75.28	0.03	3.21	1.60	0.19	1.20	100.00
96TOK-I-9L	4.13	0.33	14.00	75.15	0.06	3.14	1.56	0.32	1.31	100.00
AVG	**4.09**	**0.35**	**13.83**	**75.51**	**0.05**	**3.11**	**1.59**	**0.23**	**1.23**	**100.00**
STDDEV	**0.12**	**0.03**	**0.16**	**0.25**	**0.02**	**0.11**	**0.04**	**0.10**	**0.09**	**0.00**
n=12										

Sample: 96TOK-1-12L
December 1996

	Na20	MgO	Al203	SiO2	Cl	K20	CaO	Ti02	Fe203	Total
96TOK-1-12L	4.18	0.34	13.61	75.83	0.07	3.06	1.58	0.27	1.06	100.00
96TOK-1-12L	4.10	0.34	13.53	75.80	0.03	3.18	1.60	0.23	1.19	100.00
96TOK-1-12L	4.15	0.37	14.04	75.59	0.02	3.15	1.51	0.05	1.11	100.00
96TOK-1-12L	4.05	0.32	13.83	75.54	0.05	3.14	1.59	0.21	1.25	100.00
96TOK-1-12L	4.29	0.35	13.95	75.42	0.03	2.97	1.50	0.32	1.18	100.00
96TOK-1-12L	4.14	0.35	13.76	75.35	0.07	3.12	1.54	0.44	1.22	100.00
96TOK-1-12L	4.27	0.39	13.84	75.32	0.02	3.26	1.62	0.14	1.13	100.00
96TOK-1-12L	4.10	0.36	13.86	75.03	0.03	3.29	1.56	0.39	1.36	100.00
AVG	**4.16**	**0.35**	**13.80**	**75.49**	**0.04**	**3.15**	**1.56**	**0.26**	**1.19**	**100.00**
STDDEV	**0.08**	**0.02**	**0.17**	**0.26**	**0.02**	**0.10**	**0.04**	**0.13**	**0.09**	**0.00**
n=8										

Sample: 96TOK-1-13L
December 1996

	Na20	MgO	Al203	SiO2	Cl	K20	CaO	Ti02	Fe203	Total
96TOK-1-13L	3.81	0.37	13.10	76.52	0.02	3.21	1.58	0.19	1.20	100.00
96TOK-1-13L	3.94	0.40	13.55	76.04	0.05	3.29	1.54	0.16	1.03	100.00
96TOK-1-13L	3.97	0.35	13.75	76.00	0.09	2.98	1.55	0.11	1.20	100.00
96TOK-1-13L	3.97	0.31	13.55	75.78	0.03	3.26	1.59	0.31	1.20	100.00
96TOK-1-13L	3.96	0.37	13.70	75.78	0.04	3.13	1.55	0.27	1.19	100.00
96TOK-1-13L	4.09	0.30	13.80	75.76	0.03	3.18	1.52	0.00	1.31	100.00
96TOK-1-13L	4.32	0.31	13.41	75.75	0.06	3.27	1.44	0.31	1.13	100.00
96TOK-1-13L	3.90	0.33	13.95	75.35	0.02	3.16	1.75	0.30	1.24	100.00
AVG	**4.00**	**0.34**	**13.60**	**75.87**	**0.04**	**3.19**	**1.57**	**0.21**	**1.19**	**100.00**
STDDEV	**0.14**	**0.03**	**0.25**	**0.31**	**0.02**	**0.09**	**0.08**	**0.11**	**0.08**	**0.00**
n=8										

Appendix II: continued

Sample: 96TOK-1-20L
December 1996

	Na20	MgO	Al203	Si02	Cl	K20	CaO	TiO2	Fe203	Total
96TOK-1-20L	4.02	0.36	14.42	75.25	0.01	2.67	1.61	0.47	1.21	100.00
96TOK-1-20L	4.04	0.62	13.87	74.97	0.06	3.01	1.78	0.16	1.49	100.00
96TOK-1-20L	4.33	0.43	14.31	74.93	0.06	2.73	1.78	0.29	1.15	100.00
96TOK-1-20L	4.21	0.48	14.46	74.90	0.03	3.10	1.66	0.31	0.85	100.00
96TOK-1-20L	4.22	0.43	14.28	74.83	0.04	3.17	1.80	0.08	1.16	100.00
96TOK-1-20L	4.20	0.39	14.40	74.74	0.10	2.91	1.71	0.34	1.21	100.00
96TOK-1-20L	4.29	0.45	14.69	74.36	0.03	3.07	1.80	0.21	1.10	100.00
AVG	**4.19**	**0.45**	**14.35**	**74.85**	**0.05**	**2.95**	**1.73**	**0.27**	**1.17**	**100.00**
STDDEV	**0.11**	**0.08**	**0.23**	**0.25**	**0.03**	**0.18**	**0.07**	**0.12**	**0.17**	**0.00**
n=7										

Sample: 96TOK-1-21L
December 1996

	Na20	MgO	Al203	Si02	Cl	K20	CaO	Ti02	Fe203	Total
96TOK-1-21L	4.26	0.61	14.54	74.09	0.05	2.80	2.09	0.16	1.39	100.00
96TOK-1-21L	4.65	0.56	14.75	73.90	0.02	2.70	1.95	0.10	1.35	100.00
96TOK-1-21L	4.48	0.49	14.79	73.73	0.07	2.82	1.90	0.33	1.40	100.00
96TOK-1-21L	4.32	0.57	14.95	73.68	0.01	2.89	1.91	0.26	1.41	100.00
96TOK-1-21L	4.57	0.49	15.00	73.66	0.03	2.64	1.92	0.36	1.33	100.00
96TOK-1-21L	4.59	0.52	14.62	73.64	0.03	2.82	1.98	0.35	1.47	100.00
96TOK-1-21L	4.54	0.56	15.11	73.62	0.01	2.63	1.91	0.23	1.40	100.00
96TOK-1-21L	4.16	0.53	14.81	73.57	0.05	2.77	2.10	0.40	1.62	100.00
96TOK-1-21L	4.53	0.55	14.97	73.42	0.04	2.74	2.06	0.29	1.40	100.00
96TOK-1-21L	4.51	0.52	15.08	73.31	0.00	2.70	1.97	0.50	1.40	100.00
96TOK-1-21L	4.31	0.62	15.11	73.11	0.02	2.79	2.08	0.34	1.61	100.00
96TOK-1-21L	4.66	0.50	15.23	72.94	0.00	2.63	1.93	0.54	1.57	100.00
96TOK-1-21L	4.56	0.48	15.00	72.84	0.02	2.90	1.91	0.63	1.66	100.00
96TOK-1-21L	4.78	0.50	15.32	72.62	0.06	2.60	2.07	0.41	1.65	100.00
96TOK-1-21L	4.38	0.80	15.38	72.38	0.06	2.72	2.15	0.45	1.67	100.00
96TOK-1-21L	4.62	0.52	15.87	72.36	0.01	2.40	2.52	0.10	1.59	100.00
96TOK-1-21L	4.63	0.48	16.02	72.25	0.00	2.44	2.74	0.15	1.28	100.00
AVG	**4.50**	**0.55**	**15.09**	**73.24**	**0.03**	**2.71**	**2.07**	**0.33**	**1.48**	**100.00**
STDDEV	**0.16**	**0.08**	**0.38**	**0.56**	**0.02**	**0.14**	**0.22**	**0.15**	**0.13**	**0.00**
n =17										

Sample: 96TOK-1-22
April 1997

	Na20	MgO	Al203	Si02	Cl	K20	CaO	Ti02	Fe203	Total
96TOK-1-22	3.66	0.34	12.75	75.47	0.30	3.71	1.53	0.31	1.92	100.00
96TOK-1-22	3.53	0.30	12.66	75.44	0.36	3.98	1.43	0.49	1.81	100.00
96TOK-1-22	3.61	0.31	12.76	75.38	0.33	4.00	1.56	0.30	1.76	100.00
96TOK-1-22	3.88	0.33	12.89	75.34	0.26	3.51	1.54	0.51	1.75	100.00
96TOK-1-22	3.60	0.31	12.78	75.27	0.27	3.94	1.42	0.57	1.83	100.00
96TOK-1-22	3.70	0.31	13.38	75.07	0.25	3.73	1.41	0.19	1.96	100.00
AVG	**3.66**	**0.32**	**12.87**	**75.33**	**0.30**	**3.81**	**1.48**	**0.40**	**1.84**	**100.00**
STDDEV	**0.11**	**0.01**	**0.24**	**0.13**	**0.04**	**0.18**	**0.06**	**0.14**	**0.08**	**0.00**
n=6										

Appendix II: continued

Sample: 96TOK1-23
April 1997

	Na20	MgO	Al203	Si02	Cl	K20	CaO	Ti02	Fe203	Total
96TOK-1-23	4.23	0.16	13.48	76.64	0.04	3.24	1.58	0.03	0.59	100.00
96TOK-1-23	4.32	0.14	13.77	76.25	0.03	3.32	1.24	0.22	0.71	100.00
96TOK-1-23	4.22	0.47	14.69	74.84	0.00	2.88	1.57	0.10	1.22	100.00
96TOK-1-23	4.43	0.41	14.49	74.51	0.00	3.02	1.65	0.18	1.30	100.00
96TOK-1-23	4.17	0.48	14.85	74.12	0.04	2.82	2.07	0.11	1.34	100.00
96TOK-1-23	4.96	0.25	14.90	74.10	0.01	2.72	1.75	0.28	1.03	100.00
96TOK-1-23	4.42	0.55	15.33	73.54	0.04	2.65	1.93	0.23	1.31	100.00
AVG	**4.39**	**0.35**	**14.50**	**74.86**	**0.02**	**2.95**	**1.68**	**0.16**	**1.07**	**100.00**
STDDEV	**0.25**	**0.15**	**0.61**	**1.08**	**0.02**	**0.24**	**0.25**	**0.08**	**0.28**	**0.00**
n=7										

Tetlin Tephra (96TOK1-9, 96TOK1-12, 96TOK1-13)

Tetlin Tephra

Sample	Na20	MgO	Al203	Si02	Cl	K20	CaO	Ti02	Fe203	Total
96TOK-1-13L	3.81	0.37	13.10	76.52	0.02	3.21	1.58	0.19	1.20	100.00
96TOK-1-13L	3.94	0.40	13.55	76.04	0.05	3.29	1.54	0.16	1.03	100.00
96TOK-1-13L	3.97	0.35	13.75	76.00	0.09	2.98	1.55	0.11	1.20	100.00
96TOK-I-9L	4.07	0.32	13.52	75.93	0.03	3.13	1.62	0.21	1.17	100.00
96TOK-I-9L	3.94	0.34	13.66	75.91	0.04	3.12	1.59	0.21	1.18	100.00
96TOK-I-9L	3.96	0.34	13.78	75.84	0.10	2.81	1.62	0.21	1.34	100.00
96TOK-1-12L	4.18	0.34	13.61	75.83	0.07	3.06	1.58	0.27	1.06	100.00
96TOK-1-12L	4.10	0.34	13.53	75.80	0.03	3.18	1.60	0.23	1.19	100.00
96TOK-1-13L	3.97	0.31	13.55	75.78	0.03	3.26	1.59	0.31	1.20	100.00
96TOK-1-13L	3.96	0.37	13.70	75.78	0.04	3.13	1.55	0.27	1.19	100.00
96TOK-1-13L	4.09	0.30	13.80	75.76	0.03	3.18	1.52	0.00	1.31	100.00
96TOK-1-13L	4.32	0.31	13.41	75.75	0.06	3.27	1.44	0.31	1.13	100.00
96TOK-I-9L	4.07	0.35	13.86	75.65	0.03	3.15	1.50	0.23	1.14	100.00
96TOK-1-12L	4.15	0.37	14.04	75.59	0.02	3.15	1.51	0.05	1.11	100.00
96TOK-1-12L	4.05	0.32	13.83	75.54	0.05	3.14	1.59	0.21	1.25	100.00
96TOK-I-9L	4.17	0.33	13.96	75.51	0.02	3.20	1.57	0.19	1.04	100.00
96TOK-I-9L	4.00	0.32	13.77	75.46	0.05	3.24	1.65	0.15	1.36	100.00
96TOK-I-9L	4.10	0.39	13.81	75.42	0.05	3.15	1.63	0.21	1.23	100.00
96TOK-1-12L	4.29	0.35	13.95	75.42	0.03	2.97	1.50	0.32	1.18	100.00
96TOK-I-9L	4.39	0.42	13.83	75.36	0.04	2.97	1.60	0.08	1.31	100.00
96TOK-1-12L	4.14	0.35	13.76	75.35	0.07	3.12	1.54	0.44	1.22	100.00
96TOK-1-13L	3.90	0.33	13.95	75.35	0.02	3.16	1.75	0.30	1.24	100.00
96TOK-I-9L	3.97	0.39	14.12	75.34	0.04	3.19	1.58	0.22	1.15	100.00
96TOK-1-12L	4.27	0.39	13.84	75.32	0.02	3.26	1.62	0.14	1.13	100.00
96TOK-I-9L	4.22	0.31	13.69	75.31	0.05	3.06	1.61	0.49	1.27	100.00
96TOK-I-9L	4.10	0.39	14.01	75.28	0.03	3.21	1.60	0.19	1.20	100.00
96TOK-I-9L	4.13	0.33	14.00	75.15	0.06	3.14	1.56	0.32	1.31	100.00
96TOK-1-12L	4.10	0.36	13.86	75.03	0.03	3.29	1.56	0.39	1.36	100.00
AVG	**4.08**	**0.35**	**13.76**	**75.61**	**0.04**	**3.14**	**1.58**	**0.23**	**1.20**	**100.00**
STDDEV	**0.14**	**0.03**	**0.22**	**0.32**	**0.02**	**0.11**	**0.06**	**0.11**	**0.09**	**0.00**
n=28										

Appendix III: Hornblende and Plagioclase Crystal Chemistry

Hornblende Wt. % Oxide Data. Label Convention: HBL1 = Hornblende grain 1; -1 = edge, -2 = midpoint, -3 = center

Label	F	Na Oxide	Mg Oxide	Al Oxide	Si Oxide	Cl	K Oxide	Ca Oxide	Ti Oxide	Mn Oxide	Fe Oxide	H Oxide	Total Oxide
HBL1-1	0.000	1.750	13.803	11.135	44.797	0.047	0.397	10.199	1.072	0.316	14.426	2.030	99.972
HBL1-2	0.145	1.793	13.780	11.379	44.520	0.030	0.360	10.004	1.028	0.425	14.756	1.962	100.182
HBL1-3	0.000	1.756	13.633	11.367	44.805	0.003	0.330	10.071	0.896	0.433	15.258	2.049	100.601
HBL2-1	0.000	1.661	14.070	10.067	47.018	0.008	0.318	10.077	0.809	0.370	13.679	2.062	100.139
HBL2-2	0.000	1.631	13.761	10.256	45.724	0.025	0.297	10.153	1.292	0.407	14.296	2.040	99.882
HBL2-3	0.000	1.579	13.695	10.376	45.472	0.011	0.383	10.346	1.203	0.380	13.739	2.033	99.217
HBL3-1	0.074	1.650	13.858	10.410	45.556	0.039	0.352	9.992	0.899	0.426	13.740	1.986	98.982
HBL3-2	0.146	1.685	14.186	10.605	46.041	0.028	0.332	10.431	0.833	0.371	14.026	1.984	100.668
HBL3-3	0.148	1.637	13.763	10.787	45.302	0.042	0.355	10.037	1.098	0.390	14.255	1.958	99.772
HBL4-1	0.337	1.592	14.022	9.459	45.639	0.042	0.333	10.387	1.737	0.281	13.001	1.850	98.680
HBL4-2	0.370	1.540	14.391	9.946	45.966	0.025	0.305	9.816	0.769	0.490	13.964	1.849	99.431
HBL4-3	0.187	1.789	13.981	10.631	45.616	0.069	0.319	9.923	1.452	0.391	13.545	1.939	99.842
HBL5-1	0.000	1.971	12.337	13.097	41.993	0.033	0.774	11.105	2.478	0.172	14.499	2.023	100.482
HBL5-2	0.000	1.542	14.789	9.811	45.947	0.044	0.376	10.414	1.387	0.182	12.547	2.034	99.073
HBL5-3	0.189	2.312	13.561	14.920	40.792	0.000	0.878	11.066	3.000	0.137	11.048	1.949	99.852
HBL6-1	0.000	1.767	14.458	10.014	45.776	0.047	0.450	10.485	1.521	0.382	13.086	2.042	100.028
HBL6-2	0.514	1.704	14.289	9.921	46.271	0.033	0.418	10.448	1.562	0.272	13.495	1.801	100.728
HBL7-2	0.333	2.089	13.261	11.904	42.995	0.050	0.496	11.268	2.529	0.145	13.564	1.862	100.496
HBL8-1	0.000	1.623	14.712	9.177	46.770	0.014	0.335	10.263	1.320	0.309	13.044	2.051	99.618
HBL8-2	0.147	1.425	14.875	9.023	47.358	0.022	0.260	10.612	1.144	0.472	13.636	1.998	100.972
HBL8-3	0.478	1.452	14.799	8.855	46.920	0.031	0.260	10.395	1.101	0.191	12.954	1.801	99.237
HBL9-1	0.184	1.647	14.363	9.675	46.484	0.053	0.413	10.659	1.541	0.227	13.610	1.963	100.819
HBL9-2	0.110	1.389	15.442	8.557	47.582	0.014	0.299	10.362	1.299	0.390	12.411	2.009	99.864
HBL9-3	0.221	1.529	15.415	8.695	47.524	0.028	0.294	10.049	1.145	0.391	12.893	1.952	100.136
HBL10-1	0.000	1.949	13.501	11.050	44.680	0.039	0.345	10.161	1.168	0.418	13.273	2.013	98.597
HBL10-2	0.037	1.879	13.313	11.740	44.012	0.036	0.456	10.649	1.474	0.163	14.395	2.013	100.167
HBL10-3	0.147	1.659	14.011	10.387	45.158	0.025	0.242	9.797	0.926	0.518	14.112	1.947	98.929
HBL11-1	0.000	1.573	14.101	10.486	44.958	0.017	0.293	10.094	1.166	0.336	13.467	2.020	98.511
HBL11-2	0.368	1.607	14.381	10.049	45.055	0.011	0.270	10.089	0.991	0.291	13.834	1.838	98.784
HBL11-3	0.331	1.542	14.390	9.211	47.537	0.036	0.318	10.169	0.794	0.409	13.670	1.891	100.298

Appendix III: continued

Hornblende wt. % oxide data: continued

Label	F	Na Oxide	Mg Oxide	Al Oxide	Si Oxide	Cl	K Oxide	Ca Oxide	Ti Oxide	Mn Oxide	Fe Oxide	H Oxide	Total Oxide
HBL12-1	0.147	1.540	14.904	9.345	46.686	0.003	0.266	9.729	1.102	0.509	13.163	1.977	99.371
HBL12-2	0.184	1.560	14.666	9.298	46.383	0.047	0.352	10.238	1.409	0.273	13.361	1.947	99.718
HBL12-3	0.000	1.576	14.962	8.702	46.945	0.000	0.284	10.250	1.080	0.327	13.096	2.048	99.270
HBL13-1	0.258	1.691	14.590	9.586	45.940	0.061	0.388	10.685	1.674	0.273	13.193	1.912	100.251
HBL13-2	0.184	1.885	13.701	11.323	45.306	0.025	0.324	9.985	0.992	0.418	14.153	1.955	100.251
HBL13-3	0.515	1.681	14.005	10.517	44.860	0.000	0.299	10.305	1.058	0.419	14.094	1.776	99.529
HBL14-1	0.478	1.810	14.082	10.422	45.306	0.011	0.387	10.347	1.520	0.336	13.148	1.803	99.650
HBL14-2	0.258	1.767	14.257	9.995	46.399	0.031	0.253	10.213	1.301	0.391	13.632	1.927	100.424
HBL14-3	0.147	1.597	14.542	9.202	46.751	0.008	0.385	10.631	1.345	0.273	12.303	1.974	99.158
HBL15-1	0.147	1.875	13.988	10.661	45.468	0.020	0.297	10.409	1.235	0.382	14.011	1.978	100.471
HBL15-2	0.405	1.601	14.432	9.381	46.442	0.039	0.280	10.203	1.213	0.382	12.852	1.830	99.060
HBL15-3	0.184	1.695	14.534	9.716	46.590	0.000	0.335	9.713	0.949	0.310	13.543	1.959	99.528
AVG	0.176	1.690	14.181	10.265	45.651	0.027	0.360	10.291	1.298	0.342	13.542	1.953	99.777
STD DEV	0.159	0.178	0.591	1.211	1.389	0.018	0.121	0.345	0.459	0.098	0.741	0.080	0.653

n = 42

Appendix III: continued

Hornblende Cation Concentrations

Label	Cation F	Cation Na	Cation Mg	Cation Al	Cation Si	Cation Cl	Cation K	Cation Ca	Cation Ti	Cation Mn	Cation Fe	Cation H	Cation Total
HBL1-1	0.000	0.498	3.021	1.927	6.578	-0.011	0.074	1.605	0.118	0.039	1.772	0.000	15.621
HBL1-2	-0.061	0.511	3.021	1.972	6.548	-0.007	0.067	1.577	0.114	0.053	1.815	0.000	15.610
HBL1-3	0.000	0.498	2.973	1.960	6.555	-0.001	0.062	1.579	0.099	0.054	1.867	0.000	15.646
HBL2-1	0.000	0.468	3.046	1.723	6.828	-0.002	0.059	1.568	0.088	0.046	1.661	0.000	15.485
HBL2-2	0.000	0.463	3.006	1.771	6.700	-0.006	0.055	1.594	0.142	0.051	1.752	0.000	15.528
HBL2-3	0.000	0.451	3.006	1.801	6.697	-0.002	0.072	1.633	0.133	0.047	1.692	0.000	15.530
HBL3-1	-0.031	0.472	3.050	1.812	6.727	-0.009	0.066	1.581	0.100	0.053	1.697	0.000	15.518
HBL3-2	-0.061	0.475	3.077	1.819	6.701	-0.006	0.062	1.627	0.091	0.046	1.707	0.000	15.538
HBL3-3	-0.062	0.467	3.017	1.870	6.663	-0.009	0.067	1.582	0.121	0.049	1.753	0.000	15.518
HBL4-1	-0.142	0.458	3.102	1.655	6.775	-0.009	0.063	1.652	0.194	0.035	1.614	0.000	15.397
HBL4-2	-0.156	0.441	3.166	1.730	6.785	-0.006	0.057	1.552	0.085	0.061	1.724	0.000	15.439
HBL4-3	-0.079	0.509	3.054	1.836	6.686	-0.016	0.060	1.558	0.160	0.048	1.660	0.000	15.476
HBL5-1	0.000	0.564	2.715	2.279	6.199	-0.007	0.146	1.756	0.275	0.022	1.790	0.000	15.739
HBL5-2	0.000	0.438	3.232	1.695	6.737	-0.010	0.070	1.636	0.153	0.023	1.538	0.000	15.512
HBL5-3	-0.080	0.659	2.972	2.586	5.999	0.000	0.165	1.744	0.332	0.017	1.359	0.000	15.753
HBL6-1	0.000	0.500	3.146	1.723	6.683	-0.011	0.084	1.640	0.167	0.047	1.598	0.000	15.577
HBL6-2	-0.216	0.482	3.110	1.707	6.756	-0.008	0.078	1.635	0.171	0.034	1.648	0.000	15.397
HBL7-2	-0.140	0.597	2.916	2.070	6.342	-0.011	0.093	1.781	0.281	0.018	1.673	0.000	15.620
HBL8-1	0.000	0.459	3.200	1.578	6.825	-0.003	0.062	1.605	0.145	0.038	1.592	0.000	15.501
HBL8-2	-0.062	0.400	3.207	1.538	6.849	-0.005	0.048	1.644	0.124	0.058	1.649	0.000	15.450
HBL8-3	-0.201	0.415	3.249	1.537	6.912	-0.007	0.049	1.641	0.122	0.024	1.596	0.000	15.337
HBL9-1	-0.078	0.464	3.110	1.657	6.753	-0.012	0.077	1.659	0.168	0.028	1.654	0.000	15.480
HBL9-2	-0.046	0.391	3.342	1.464	6.908	-0.003	0.055	1.612	0.142	0.048	1.507	0.000	15.420
HBL9-3	-0.093	0.431	3.338	1.489	6.905	-0.006	0.054	1.564	0.125	0.048	1.567	0.000	15.422
HBL10-1	0.000	0.560	2.982	1.930	6.622	-0.009	0.065	1.613	0.130	0.052	1.645	0.000	15.590
HBL10-2	-0.015	0.536	2.917	2.034	6.470	-0.008	0.085	1.677	0.163	0.020	1.770	0.000	15.649
HBL10-3	-0.062	0.477	3.095	1.814	6.692	-0.006	0.046	1.556	0.103	0.065	1.749	0.000	15.529
HBL11-1	0.000	0.452	3.113	1.831	6.659	-0.004	0.055	1.602	0.130	0.042	1.668	0.000	15.548
HBL11-2	-0.155	0.464	3.190	1.762	6.704	-0.003	0.051	1.608	0.111	0.037	1.722	0.000	15.491
HBL11-3	-0.140	0.436	3.126	1.582	6.928	-0.008	0.059	1.588	0.087	0.051	1.666	0.000	15.375

Appendix III: continued

Hornblende Cation Concentrations: continued

Label	Cation F	Cation Na	Cation Mg	Cation Al	Cation Si	Cation Cl	Cation K	Cation Ca	Cation Ti	Cation Mn	Cation Fe	Cation H	Cation Total
HBL12-1	-0.062	0.437	3.253	1.613	6.837	-0.001	0.050	1.527	0.121	0.063	1.612	0.000	15.450
HBL12-2	-0.077	0.443	3.203	1.606	6.797	-0.011	0.066	1.607	0.155	0.034	1.637	0.000	15.460
HBL12-3	0.000	0.447	3.265	1.501	6.872	0.000	0.053	1.608	0.119	0.041	1.603	0.000	15.509
HBL13-1	-0.108	0.480	3.181	1.653	6.720	-0.014	0.072	1.675	0.184	0.034	1.614	0.000	15.491
HBL13-2	-0.077	0.535	2.989	1.953	6.631	-0.006	0.060	1.566	0.109	0.052	1.732	0.000	15.544
HBL13-3	-0.217	0.484	3.098	1.840	6.658	0.000	0.057	1.639	0.118	0.053	1.749	0.000	15.479
HBL14-1	-0.201	0.518	3.096	1.812	6.683	-0.003	0.073	1.635	0.169	0.042	1.622	0.000	15.446
HBL14-2	-0.109	0.500	3.097	1.717	6.763	-0.007	0.047	1.595	0.143	0.048	1.662	0.000	15.456
HBL14-3	-0.062	0.454	3.177	1.589	6.852	-0.002	0.072	1.669	0.148	0.034	1.508	0.000	15.439
HBL15-1	-0.062	0.531	3.046	1.836	6.642	-0.004	0.055	1.629	0.136	0.047	1.712	0.000	15.568
HBL15-2	-0.171	0.458	3.174	1.631	6.853	-0.009	0.053	1.613	0.135	0.048	1.586	0.000	15.371
HBL15-3	-0.078	0.482	3.173	1.677	6.825	0.000	0.063	1.524	0.105	0.038	1.659	0.000	15.468
AVG	-0.074	0.481	3.101	1.776	6.698	-0.006	0.067	1.618	0.143	0.043	1.662	0.000	15.509
STD DEV	0.067	0.051	0.121	0.214	0.184	0.004	0.023	0.055	0.051	0.012	0.093	0.000	0.092
n = 42													

Appendix III: continued

Plagioclase Wt. % Oxide Data. Label Convention: PLAG1 = Plagioclase grain 1; -1 = edge, -2 = midpoint, -3 = center

Label	Na Oxide	Al Oxide	Si Oxide	K Oxide	Ca Oxide	Fe Oxide	Total Oxide
PLAG1-1	6.605	27.504	58.703	0.342	8.433	0.100	101.687
PLAG1-2	6.551	27.479	58.360	0.306	8.619	0.061	101.376
PLAG1-3	4.656	30.105	53.463	0.160	11.989	0.100	100.473
PLAG2-1	6.352	27.463	58.286	0.275	8.411	0.143	100.930
PLAG2-2	6.354	27.905	57.744	0.268	9.036	0.222	101.529
PLAG2-3	5.588	28.632	55.383	0.117	9.681	0.247	99.648
PLAG3-1	5.894	28.211	56.365	0.241	9.720	0.210	100.641
PLAG3-2	5.539	29.096	55.991	0.173	10.205	0.159	101.163
PLAG3-3	6.185	28.192	56.187	0.286	9.421	0.102	100.373
PLAG4-1	6.082	28.127	56.981	0.224	9.291	0.206	100.911
PLAG4-2	6.497	26.853	59.542	0.366	8.043	0.304	101.605
PLAG4-3	7.016	26.791	59.278	0.317	7.907	0.436	101.745
PLAG5-1	5.671	27.802	57.422	0.298	9.534	0.308	101.035
PLAG5-2	5.461	29.286	54.993	0.137	10.671	0.477	101.025
PLAG5-3	5.479	25.330	63.268	0.698	8.051	0.479	103.305
PLAG6-1	6.061	28.386	56.792	0.258	9.425	0.033	100.955
PLAG6-2	6.582	27.469	58.387	0.251	8.480	0.233	101.402
PLAG6-3	6.185	27.820	57.635	0.266	9.072	0.349	101.327
PLAG7-1	6.446	27.279	58.212	0.263	8.462	0.247	100.909
PLAG7-2	6.230	27.662	57.394	0.255	9.331	0.177	101.049
PLAG7-3	6.045	28.072	57.094	0.233	9.566	0.316	101.326
PLAG8-1	6.808	26.736	58.372	0.340	8.401	0.204	100.861
PLAG8-2	5.319	29.147	54.527	0.196	11.068	0.161	100.418
PLAG8-3	6.176	27.873	57.816	0.286	9.162	0.351	101.664
PLAG9-1	6.415	26.994	58.044	0.253	8.789	0.257	100.752
PLAG9-2	5.339	29.468	55.343	0.139	11.036	0.224	101.549
PLAG9-3	6.522	26.768	58.492	0.289	8.278	0.239	100.588
PLAG10-1	5.606	29.076	56.037	0.184	10.530	0.304	101.737
PLAG10-2	5.756	28.382	56.578	0.213	9.625	0.255	100.809
PLAG10-3	5.966	27.995	57.479	0.236	9.462	0.230	101.368
PLAG11-1	5.931	28.172	56.236	0.259	9.348	0.165	100.111
PLAG11-2	6.103	28.058	57.564	0.288	9.244	0.153	101.410
PLAG11-3	6.073	27.841	57.057	0.241	9.160	0.194	100.566

Appendix III: continued

Plagioclase Wt. % Oxide Data: continued

Label	Na Oxide	Al Oxide	Si Oxide	K Oxide	Ca Oxide	Fe Oxide	Total Oxide
PLAG12-1	6.579	26.949	58.114	0.326	8.064	0.196	100.228
PLAG12-2	6.647	27.032	58.058	0.289	8.290	0.233	100.549
PLAG12-3	6.946	26.458	59.948	0.313	7.582	0.098	101.345
PLAG13-1	5.850	28.634	57.044	0.209	9.984	0.400	102.121
PLAG13-2	5.607	28.639	56.627	0.284	9.735	0.261	101.153
PLAG13-3	6.034	27.757	55.943	0.374	9.233	0.237	99.578
PLAG14-1	6.750	26.993	59.118	0.299	8.142	0.396	101.698
PLAG14-2	6.905	26.424	58.860	0.299	8.042	0.278	100.808
PLAG14-3	6.965	25.905	59.676	0.365	7.543	0.243	100.697
PLAG15-1	5.191	29.421	55.733	0.149	10.844	0.298	101.636
PLAG15-2	4.824	29.252	55.113	0.250	11.062	0.143	100.644
PLAG15-3	6.705	26.603	58.856	0.325	8.059	0.420	100.968
AVG	6.100	27.823	57.425	0.270	9.201	0.241	101.059
STD DEV	0.569	1.022	1.707	0.090	1.041	0.106	0.650

Appendix III: continued
Plagioclase Cation Data

Label	Cation Na	Cation Al	Cation Si	Cation K	Cation Ca	Cation Fe	Cation Total
PLAG1-1	0.564	1.426	2.583	0.019	0.398	0.003	4.993
PLAG1-2	0.561	1.430	2.577	0.017	0.408	0.002	4.995
PLAG1-3	0.406	1.597	2.407	0.009	0.578	0.003	5.000
PLAG2-1	0.545	1.434	2.581	0.016	0.399	0.005	4.980
PLAG2-2	0.544	1.453	2.551	0.015	0.428	0.007	4.998
PLAG2-3	0.488	1.521	2.496	0.007	0.467	0.008	4.987
PLAG3-1	0.510	1.485	2.517	0.014	0.465	0.007	4.998
PLAG3-2	0.477	1.524	2.488	0.010	0.486	0.005	4.990
PLAG3-3	0.537	1.488	2.517	0.016	0.452	0.003	5.013
PLAG4-1	0.524	1.474	2.534	0.013	0.443	0.007	4.995
PLAG4-2	0.554	1.391	2.617	0.021	0.379	0.010	4.972
PLAG4-3	0.598	1.389	2.607	0.018	0.373	0.014	4.999
PLAG5-1	0.488	1.454	2.549	0.017	0.453	0.010	4.971
PLAG5-2	0.473	1.542	2.456	0.008	0.511	0.016	5.006
PLAG5-3	0.456	1.282	2.718	0.038	0.371	0.015	4.880
PLAG6-1	0.522	1.487	2.525	0.015	0.449	0.001	4.999
PLAG6-2	0.563	1.429	2.577	0.014	0.401	0.008	4.992
PLAG6-3	0.531	1.451	2.551	0.015	0.430	0.012	4.990
PLAG7-1	0.554	1.426	2.581	0.015	0.402	0.008	4.986
PLAG7-2	0.537	1.448	2.550	0.014	0.444	0.006	4.999
PLAG7-3	0.520	1.467	2.531	0.013	0.454	0.011	4.996
PLAG8-1	0.586	1.400	2.594	0.019	0.400	0.007	5.006
PLAG8-2	0.464	1.545	2.452	0.011	0.533	0.005	5.010
PLAG8-3	0.528	1.450	2.551	0.016	0.433	0.012	4.990
PLAG9-1	0.553	1.415	2.581	0.014	0.419	0.009	4.991
PLAG9-2	0.460	1.543	2.458	0.008	0.525	0.007	5.001
PLAG9-3	0.562	1.403	2.600	0.016	0.394	0.008	4.983
PLAG10-1	0.481	1.518	2.482	0.010	0.500	0.010	5.001
PLAG10-2	0.497	1.490	2.520	0.012	0.459	0.009	4.987
PLAG10-3	0.512	1.460	2.544	0.013	0.449	0.008	4.986
PLAG11-1	0.516	1.489	2.522	0.015	0.449	0.006	4.997
PLAG11-2	0.523	1.462	2.546	0.016	0.438	0.005	4.990
PLAG11-3	0.525	1.463	2.544	0.014	0.438	0.007	4.991

Appendix III: continued

Plagioclase Cation Data: continued

Label	Cation Na	Cation Al	Cation Si	Cation K	Cation Ca	Cation Fe	Cation Total
PLAG12-1	0.569	1.417	2.593	0.019	0.385	0.007	4.990
PLAG12-2	0.574	1.419	2.585	0.016	0.395	0.008	4.997
PLAG12-3	0.593	1.372	2.637	0.018	0.357	0.003	4.980
PLAG13-1	0.499	1.486	2.512	0.012	0.471	0.013	4.993
PLAG13-2	0.483	1.498	2.514	0.016	0.463	0.009	4.983
PLAG13-3	0.528	1.477	2.526	0.022	0.447	0.008	5.008
PLAG14-1	0.576	1.399	2.601	0.017	0.384	0.013	4.990
PLAG14-2	0.594	1.382	2.612	0.017	0.382	0.009	4.996
PLAG14-3	0.599	1.353	2.645	0.021	0.358	0.008	4.984
PLAG15-1	0.446	1.536	2.469	0.008	0.515	0.010	4.984
PLAG15-2	0.418	1.543	2.466	0.014	0.530	0.005	4.976
PLAG15-3	0.576	1.389	2.608	0.018	0.383	0.014	4.988
AVG	0.525	1.456	2.548	0.015	0.438	0.008	4.990
STD DEV	0.048	0.061	0.060	0.005	0.051	0.004	0.019

Appendix IV: The $^{40}Ar/^{39}Ar$ Age Equation

The $^{40}Ar/^{39}Ar$ age equation:

$$t = (1/\lambda)\ln[1 + J(^{40}Ar^*/^{39}Ar_K)] \quad \text{(eqn. A.1)}$$

where

$$\lambda = 5.543 \times 10^{-10}\ yr^{-1} \qquad \text{(decay constant for } ^{40}K\text{)} \quad \text{(eqn. A.2)}$$

$$J = (e^{\lambda t} - 1)/(^{40}Ar^*/^{39}Ar_K)_{standard} \qquad (t = \text{age of standard}) \quad \text{(eqn. A.3)}$$

$$^{40}Ar^*/^{39}Ar_K = \frac{(^{40}Ar/^{39}Ar)_m - 295.5(^{36}Ar/^{39}Ar)_m + 295.5(^{36}Ar/^{37}Ar)_{Ca}(^{37}Ar/^{39}Ar)_m}{1 - (^{39}Ar/^{37}Ar)_{Ca}(^{37}Ar/^{39}Ar)_m} - (^{40}Ar/^{39}Ar)_K \quad \text{(eqn. A.4)}$$

and

$$J = (\lambda/\lambda_e)(^{39}K/^{40}K)\Delta T\int\varphi(\varepsilon)\sigma(\varepsilon)d(\varepsilon) \quad \text{(eqn. A.5)}$$

where

ΔT = length of irradiation
$\varphi(\varepsilon)$ = neutron flux density of energy ε
$\sigma(\varepsilon)$ = capture cross section of ^{39}K having energy ε

Appendix V: Mean Square Weighted Deviation Calculations for the $^{40}Ar/^{39}Ar$ Method

n	Age (ka)	+/- (ka)	running avg of mean	wi	wi * Xi	running sum of wi	running sum of wi * Xi	running mean weighted by error	running weighted avg. error	$(Xi - X)^2$	error squared	square of weighted deviations	running sum square of weighted dev.	running MSWD	critical MSWD
1	396.55	235.98	396.55	1.7958E-05	0.007121	1.79577E-05	0.0071211	396.55	235.98	185171.2426	55686.5604	3.325	3.325	0.000	
2	451.21	119.19	423.88	7.0392E-05	0.031761	8.83492E-05	0.0388825	440.10	106.39	141116.8915	14206.2561	9.933	13.259	0.698	
3	460.05	231.67	435.94	1.8632E-05	0.008572	0.000106981	0.0474541	443.57	96.68	134553.4517	53670.9889	2.507	15.766	0.830	3.828
4	476.88	237.17	446.17	1.7778E-05	0.008478	0.000124759	0.0559321	448.32	89.53	227414.5344	56249.6089	4.043	19.809	1.043	3.000
5	492.49	296.95	455.44	1.1341E-05	0.005585	0.0001361	0.0615172	452.00	85.72	111806.8298	88179.3025	1.268	21.077	1.109	2.633
6	503.19	348.06	463.40	8.2545E-06	0.004154	0.000144354	0.0656708	454.93	83.23	104765.6887	121145.7636	0.865	21.941	1.155	2.414
7	503.83	231.03	469.17	1.8735E-05	0.009439	0.00016309	0.0751102	460.55	78.30	253844.6689	53374.8609	4.756	26.697	1.405	2.265
8	553.16	262.37	479.67	1.4527E-05	0.008036	0.000177616	0.0831459	468.12	75.03	74914.58185	68838.0169	1.088	27.786	1.462	2.155
9	624.55	235.79	495.77	1.7987E-05	0.011234	0.000195603	0.0943794	482.50	71.50	40931.47367	55596.9241	0.736	28.522	1.501	2.069
10	639.37	118.96	510.13	7.0664E-05	0.045180	0.000266267	0.1395599	524.13	61.28	35154.48109	14151.4816	2.484	31.006	1.632	2.000
11	671.46	136.89	524.79	5.3365E-05	0.035832	0.000319632	0.1753923	548.73	55.93	24150.80193	18738.8721	1.289	32.295	1.700	1.943
12	748.02	149.29	543.40	4.4868E-05	0.033562	0.0003645	0.2089546	573.26	52.38	6216.578626	22287.5041	0.279	32.574	1.714	1.894
13	796.22	291.61	562.84	1.176E-05	0.009363	0.00037626	0.2183179	580.23	51.55	939.1333603	85036.3921	0.011	32.585	1.715	1.853
14	877.44	179.69	585.32	3.0971E-05	0.027175	0.000407231	0.2454929	602.84	49.55	2557.802016	32288.4961	0.079	32.664	1.719	1.816
15	925.89	215.02	608.02	2.1629E-05	0.020026	0.00042886	0.2655193	619.13	48.29	9805.894609	46233.6004	0.212	32.876	1.730	1.784
16	945.53	297.54	629.12	1.1296E-05	0.010680	0.000440156	0.2761996	627.50	47.66	14081.3151	88530.0516	0.159	33.035	1.739	1.756
17	*961.3*	*288.79*	*648.65*	*1.199E-05*	*0.011526*	*0.000452146*	*0.2877257*	*636.36*	*47.03*	*18064.62799*	*83399.6641*	*0.217*	*33.252*	*1.750*	*1.730*
18	*968.8*	*297.84*	*666.44*	*1.127E-05*	*0.010921*	*0.000463419*	*0.2986469*	*644.44*	*46.45*	*20148.30273*	*88708.6656*	*0.227*	*33.479*	*1.762*	*1.707*
19	*1189*	*74.03*	*693.92*	*0.0001825*	*0.216869*	*0.000645886*	*0.5155163*	*798.15*	*39.35*	*130808.601*	*5480.4409*	*23.868*	*57.347*	*3.018*	*1.686*
20	*1283*	*156.86*	*723.38*	*4.064E-05*	*0.052150*	*0.000686528*	*0.5676662*	*826.87*	*38.17*	*208195.7431*	*24605.0596*	*8.462*	*65.809*	*3.464*	*1.667*

Age is calculated at n=16, where the MSWD > ciritcal MSWD

		weighted avg	
MSWD	**0.73**	**error (ka)**	**47.66**
sq root MSWD	**0.85**		
modified error	**40.59**	**mean age (ka)**	**627.50**

MSWD is less than one, so don't use modified error.

Final age of hornblende in Tetlin Tephra (96TOK1-9) is 627.5 +/- 47.7 ka

Appendix VI: Argon Isotopic Data

Tetlin Tephra (sample 96TOK1-9)

UAF Sample ID: UAF071-03 96TOK-1-9 HO#1 08-11-98

Weighted average of J from standards = 0.000257 +/- 0.000001

Run	40Ar/39Ar measured	+/-	37Ar/39Ar measured	+/-	36Ar/39Ar measured	+/-	% Atmospheric 40Ar	Ca/K	+/-	Cl/K	+/-	40*/39K	+/-	Age (ka)	+/- (ka)
1	118.22959	1.12115	8.77940	0.12062	0.39526	0.00427	98.25559	16.202	0.224	0.065	0.001	2.07377	0.62318	961.27	288.79
2	48.98233	0.32167	8.41280	0.08747	0.16415	0.00270	97.79495	15.521	0.162	0.062	0.001	1.08540	0.75088	503.19	348.06
3	44.28272	0.22236	10.76235	0.05784	0.14707	0.00130	96.37930	19.887	0.108	0.115	0.001	1.61362	0.32211	748.02	149.29
4	71.41911	0.14850	8.69010	0.03688	0.24052	0.00097	98.64441	16.036	0.068	0.100	0.001	0.97327	0.25714	451.21	119.19
5	66.01291	0.33821	8.27766	0.05119	0.22052	0.00145	97.81671	15.271	0.095	0.080	0.001	1.44843	0.29535	671.46	136.89
6	76.33366	0.43257	8.78998	0.06599	0.25409	0.00190	97.53351	16.221	0.122	0.101	0.001	1.89289	0.38774	877.44	179.69
7	65.55888	0.44944	7.66991	0.07046	0.21667	0.00249	96.82650	14.144	0.131	0.069	0.001	2.09004	0.64271	968.81	297.84
8	65.72329	0.52057	8.67838	0.07320	0.21766	0.00275	96.91256	16.014	0.136	0.096	0.001	2.03981	0.64205	945.53	297.54
9	64.83706	0.36563	7.88420	0.08356	0.21798	0.00204	98.47668	14.541	0.155	0.086	0.001	0.99233	0.49978	460.05	231.67
10	52.13905	0.18590	8.64591	0.05336	0.17453	0.00198	97.72312	15.954	0.099	0.100	0.001	1.19321	0.56605	553.16	262.37
11	53.03873	0.14121	8.97044	0.02723	0.17821	0.00175	98.07084	16.556	0.051	0.106	0.001	1.02866	0.51164	476.88	237.17
12	71.38704	0.24007	9.40439	0.06656	0.24030	0.00228	98.52041	17.362	0.124	0.107	0.001	1.06232	0.64061	492.49	296.95
13	77.79078	0.37800	8.27792	0.05668	0.26238	0.00213	98.90598	15.271	0.105	0.082	0.001	0.85534	0.50905	396.55	235.98
14	72.05661	0.59353	8.24504	0.07227	0.23653	0.00225	96.17711	15.210	0.134	0.087	0.001	2.76842	0.33856	1283.15	156.86
15	61.94454	0.20615	8.99517	0.04714	0.20509	0.00170	96.79285	16.602	0.088	0.102	0.001	1.99743	0.46399	925.89	215.02
16	70.96136	0.30600	8.49916	0.04779	0.23756	0.00127	98.06637	15.682	0.089	0.093	0.001	1.37921	0.25666	639.37	118.96
17	90.63945	0.62238	8.74482	0.06019	0.30308	0.00202	98.11519	16.137	0.112	0.098	0.001	1.71762	0.62920	796.22	291.61

UAF Sample ID: UAF065-41 96TOK-1-9 HO 06-20-97

Weighted average of J from standards = 0.000248 +/- 0.000001

18	43.11937	0.23275	10.26087	0.06677	0.13951	0.00089	93.88620	18.954	0.124	0.083	0.001	2.65221	0.16526	1188.54	74.03
19	32.98574	0.18503	10.05796	0.08354	0.10940	0.00185	95.79957	18.577	0.155	0.083	0.001	1.39347	0.52617	624.55	235.79
20	21.64402	0.39249	10.23973	0.15877	0.07197	0.00162	94.83430	18.915	0.295	0.083	0.001	1.12409	0.51552	503.83	231.03